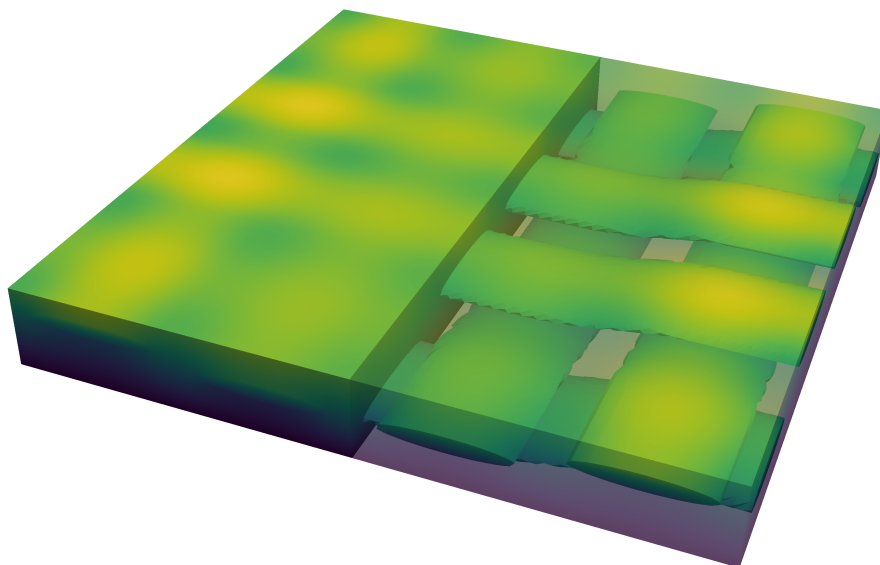


Department of Precision and Microsystems Engineering

A Generalized Finite Element Method with Spread and Discrete Enrichments for Capturing High Thermal Gradients in Composites

Zhiyuan Xu

Report no : 2021.093
Coach : Dr. Alejandro M. Aragón
Specialisation : Engineering Mechanics
Type of report : Master of Science Thesis
Date : 29 November 2021



A Generalized Finite Element Method with Spread and Discrete Enrichments for Capturing High Thermal Gradients in Composites

by

Zhiyuan XU

to obtain the degree of Master of Science
in Mechanical Engineering
at the Delft University of Technology,
to be defended on Monday November 29, 2021.

An electronic version of this dissertation is available at
<http://repository.tudelft.nl/>.



Acknowledgements

As finishing the master thesis, my master program finally comes to an end. Looking at my last two years life in TU Delft, there are many precious moments. The experience on my thesis project “A Generalized Finite Element Method with Spread and Discrete Enrichments for Capturing High Thermal Gradients in Composites” is also valuable. The completion of my master program will not go smoothly without the assistance of some people, and I would like to acknowledge them all here.

First of all, I would like to thank my supervisor, Prof. Alejandro Aragón for the nice suggestions when I was confronted with difficulties during the thesis project. His critical academic attitudes and outstanding research skills have set an excellent example for my future work. Also, I would like to thank my group colleagues PhD senior Jian Zhang and Yuheng Yan, who gave me help when I started coding in *Hybrida*. Besides, the collaborations with other group members were also nice and I will never forget the time working with them.

Second, I would like to thank my friend Fulin Yang who is also studying in Department of Precision and Microsystems Engineering. He and I often play sports together to refresh ourselves, which is an indispensable part of lives. Also, I would like to thank all my friends for learning together and making the life fun.

Last, I would like to give my great gratitude to my parents for their encouragement and support. They always give me confidence when I am depressed.

Zhiyuan Xu
Delft, November 2021

Abstract

The demand for composites is rising in industries for instance, in aircraft and automobile engines. In these applications, composites encounter high thermal gradients service condition, and composites exhibit material discontinuous gradient field. It is essential to study how high thermal gradients and material discontinuities influence on the composites' behavior. Composites are usually modelled with the standard finite element method (FEM), but mesh refinement is required near material interfaces and regions with high thermal gradients to obtain accurate solutions. Enriched finite element procedures are able to solve this issue. The Generalized Finite Element Method (GFEM) can approximate high thermal gradients by adding enriched degrees of freedom (DOFs) to original mesh nodes. In addition, the Interface-enriched Generalized Finite Element Method (IGFEM) can cope with material discontinuities by creating nodes at the intersection between discontinuities and edges of elements in the mesh. Yet, GFEM and IGFEM have their own limitations when implemented: while GFEM needs extra enrichments to resolve the material interfaces in composites, and IGFEM requires mesh refinement if thermal gradients are too high in cut elements. Then we can combine the best of both methods.

In this thesis, a new Generalized Finite Element Method with spread and discrete enrichments (GFEM^{sd}) is developed to simulate heat transfer problems with high thermal gradients in composites. By combining GFEM and IGFEM formulations, GFEM^{sd} is capable of dealing with high thermal gradients and material discontinuities simultaneously in an effective manner. We show that GFEM^{sd} obtains accurate results when compared with analytical solutions in numerical examples. A convergence study illustrates that fewer DOFs are required in GFEM^{sd} for achieving the same level of accuracy comparable to that of IGFEM. We then apply GFEM^{sd} to simulate a twill pattern composite and derive effective heat conductivity values. Lastly, based on the composite's minimum effective heat conductivity, fiber shape optimization is conducted to obtain the best design for a fixed fiber volume fraction.

Contents

Acknowledgements	i
Abstract	iii
1 Introduction	1
2 A Generalized Finite Element Method with Spread and Discrete Enrichments for Capturing High Thermal Gradients in Composites	3
2.1 Problem Description	3
2.2 GFEM ^{sd} Formulation	5
2.3 Comparison of GFEM ^{sd} , IGFEM and GFEM	7
2.4 Numerical Examples	7
2.4.1 One-Dimensional Heat Source Conduction Problem	7
2.4.2 Two-Dimensional Source Heat Conduction Problem	9
2.4.3 Multiple Curved Material Interfaces	11
2.5 Three-Dimensional Twill Pattern Composite	13
2.5.1 Three-Dimensional Twill Pattern Composite Geometric Modelling	13
2.5.2 Effective Heat Conductivity and Boundary Conditions of the RVE Model	15
2.5.3 Fiber Shape Optimization of the RVE Model	16
2.6 Conclusion	18
3 Reflection	19
3.1 Choice of Research Project	19
3.2 Process of The Project.	19
3.3 Personal Improvement during The Project	20
3.4 Future Work Prospections.	20
A Enriched Finite Element Methods	21
A.1 Generalized Finite Element Method	21
A.2 Interface-enriched Generalized Finite Element Method	21
B Mathematical Equation of The Twill Composite Fiber Centerline	23
C Analytic Effective Heat Conductivity of A Simple Cubic Composite Model	25
D The Fiber Volume with A Cosine Function Centerline	27
E Parameters Mapping of Twill Composite Model Effective Heat Conductivity	29
References	31

1

Introduction

Composites are increasingly popular in engineering, including aerospace [1], civil engineering [2], maritime engineering [3], and automotive [4] because of their high specific strength, stiffness, and long service life. In these applications, composite materials are often exposed to high temperatures, for instance in rocket nozzles [5], thermal protection systems in aircraft where the temperature usually exceeds 1000 °C [6], and automobile engines [7]. Among composite materials, ceramic matrix composites (CMCs) have been regarded as promising candidate materials for the mentioned components because of their low thermal conductivity, light weight, and high strength to meet severe service demands [8]. However, under high temperatures, the composite's thermal and mechanical properties are strongly affected, which limits their applicability. Large temperature differences and inhomogenous heat distribution in a manufactured part could lead to failure [9], inner stress concentration [10], and microcracks [11, 12]. For example, a heat load may cause distortion of the composite geometry during operation [13], and cyclic thermal shocks and long-term thermal aging will affect the mechanical properties of composite structures [14, 15]. These heat-induced concerns pose both safety and economic issues in the composite engineering practice. Therefore, to achieve better thermal performance, it is desirable to exploit methods that faithfully predict heat distribution to design the composite structures. And although experiments could be conducted to that end, they are expensive and time-consuming. Numerical methods, on the other hand, are a wise alternative to experiments and are the focus of this thesis.

The classic way to simulate heat conduction in composites is using Finite Element Method (FEM) [16–18]. By using mesh refinement [19, 20] and geometry-conforming meshes [21], that is, meshes fitted to material interfaces, the temperature field with high thermal gradients in composites can be simulated accurately. However, this technique is computationally expensive because very fine meshes should be generated to capture high gradients. In addition, composites contain two or more material phases, so fine meshes or high-order elements are also needed near the material discontinuities to get accurate solutions.

The Generalized Finite Element Method (GFEM) [22], which incorporates a *priori* knowledge of the solution field in the form of enrichment functions into the formulation, could avoid mesh refinement by enriching the finite element space. In [23] and [24], O'Hara *et al.* proposed a GFEM formulation with global–local enrichments for steady-state and transient heat transfer problems, respectively. Their formulations can capture sharp thermal gradients reasonably with coarse, uniform meshes, but the iterative process to obtain the final local enrichment is tedious. Abbas *et al.* [25] adopted a set of regularized Heaviside functions as enrichments to solve convection-dominated problems involving solutions with high thermal gradients. A set of enrichments were chosen when one enrichment was insufficient to represent high thermal gradients. The inconvenience of this approach is that several enrichments complicate the implementation. Using parametric enrichments in GFEM is another method to resolve high gradients. Waisman *et al.* [26] defined *a-posteriori* energy form residual error, and minimized it adaptively to determine the parameters of the enrichment function and capture high gradients. Later, Zeller *et al.* [27] and Iqbal *et al.* [28] adopted similar concepts to modify the parameterized enrichment functions by using other form of residual error measures.

Different from GFEM, the Interface-enriched Generalized Finite Element Method (IGFEM) [29] creates en-

riched nodes directly at the intersection between material interfaces and edges of mesh elements, and enriched degrees of freedom are added to those nodes. IGFEM was designed to solve problems with weak discontinuity, where the gradient field is discontinuous, by a straightforward computer implementation. With this aim, the contributions of IGFEM are found in many areas, including for instance, the modelling of in-plane deformations in heterogeneous adhesives [30], the transverse failure of composite laminates [31, 32], the shape optimization of microvascular composite panels [33], and the topology optimization for compliance minimization problems [34]. In the context of heat transfer problems, two-dimensional (2D) multiple materials [29] and three-dimensional (3D) composite models with complex internal morphologies such as woven microvascular composites were also investigated [35–38].

One important material property of composites is the thermal conductivity. Thermal conductivity determines the conduction capability of composites, and plays a critical role in the composites' thermal behavior, which has also been studied extensively [39, 40]. Gori *et al.* [41] evaluated the thermal conductivity of composite material by theoretical method with a cubic cell, and compared with numerical results. Gou *et al.* [42] presented a numerical approach based on homogenization for predicting the effective thermal conductivities of plain woven composites. Zhou *et al.* [43] established a parametric formulations between the architecture of fiber reinforcement and effective thermal conductivity, which were predicted by using an analytical homogenization method. Composites' thermal conductivity was also optimized with regards to their microstructure. Yan *et al.* [44] optimized the thermal conductivity of a UO_2 -Mo composite by tailoring the Mo channel structural characteristics using machine learning. By adopting genetic algorithm, Liu *et al.* [45] developed the geometric optimization of aerogel composite to minimize effective thermal conductivity. Yin *et al.* [46] employed particle swarm optimization algorithm to optimize the composite parameters, and obtained the minimized thermal conductivity.

This present work has two major objectives : (i) to develop a new Generalized Finite Element Method with spread and discrete enrichment (GFEM^{sd}) which combines the formulations of GFEM and IGFEM to solve composite heat transfer problems with high thermal gradients, and (ii) to apply the proposed method to the gradient-based design of embedded fibers in a CMCs plate. For the former, numerical examples with analytical solutions are compared with the GFEM^{sd} numerical results, showing that GFEM^{sd} can capture the temperature field accurately. Convergence study of these examples are shown and compared with IGFEM reference results, GFEM^{sd} converges faster than IGFEM, and is more accurate than IGFEM. For the latter, we focus on the twill pattern composite model, the effective heat conductivity of the model using GFEM^{sd} is derived. Furthermore, a scheme for the fiber shape optimization to obtain minimal effective heat conductivity is conducted, giving the best fiber shape design for a fixed fiber volume.

2

A Generalized Finite Element Method with Spread and Discrete Enrichments for Capturing High Thermal Gradients in Composites

In this chapter, the formulation of the proposed GFEM^{sd} algorithm is elaborated in detail. Then 2D numerical examples are presented to verify the method's accuracy. Finally, GFEM^{sd} formulation is expanded to solve 3D composite problem.

2.1. Problem Description

Consider an open domain $\Omega \subset \mathbb{R}^d$ referenced by a Cartesian coordinate system spanned by base vectors $\{\mathbf{e}_i\}_{i=1}^d$ as illustrated in Figure 2.1. This domain composes of two mutually exclusive material regions Ω_1 and Ω_2 , with closure $\bar{\Omega}$, such that $\Omega = \Omega_1 \cup \Omega_2 \subset \mathbb{R}^d$, $\Omega_1 \cap \Omega_2 = \emptyset$. The phase interface Γ_{12} separates the two sub-domain Ω_1 and Ω_2 . The external boundary $\Gamma = \bar{\Omega} - \Omega$ has outward unit normal \mathbf{n} and is partitioned into three distinct boundary conditions Γ_u , Γ_q and Γ_h , which are the Dirichlet, Neumann and Robin boundary conditions, such that $\Gamma = \Gamma_u \cup \Gamma_q \cup \Gamma_h$ and $\Gamma_u \cap \Gamma_q \cap \Gamma_h = \emptyset$. The strong form for the steady-state heat boundary value problem can be written as follows: Given the heat conductivity $\boldsymbol{\kappa} : \bar{\Omega} \rightarrow \mathbb{R}^d \times \mathbb{R}^d$, the heat source $f : \Omega \rightarrow \mathbb{R}$, prescribed temperature $\bar{u} : \Gamma_u \rightarrow \mathbb{R}$, prescribed heat flux $\bar{q} : \Gamma_q \rightarrow \mathbb{R}$, and heat transfer coefficient $h : \Gamma_h \rightarrow \mathbb{R}$ and ambient temperature $u_\infty : \Gamma_h \rightarrow \mathbb{R}$, find the temperature field $u : \bar{\Omega} \rightarrow \mathbb{R}$ such that

$$\begin{aligned} \nabla \cdot (\boldsymbol{\kappa} \nabla u) + f &= 0 && \text{on } \Omega, \\ u &= \bar{u} && \text{on } \Gamma_u, \\ \boldsymbol{\kappa} \nabla u \cdot \mathbf{n} &= \bar{q} && \text{on } \Gamma_q, \\ \boldsymbol{\kappa} \nabla u \cdot \mathbf{n} &= h(u_\infty - u) && \text{on } \Gamma_h. \end{aligned} \tag{2.1}$$

Let \mathcal{U} be the set of functions for the temperature field, $\mathcal{U} \subset H^1(\bar{\Omega}) = \{u : u|_{\Gamma_u} = \bar{u}\}$ and \mathcal{V} be the variation space, $\mathcal{V} \subset H_0^1(\bar{\Omega}) = \{v : v|_{\Gamma_u} = 0\}$, the weak form of Equation (2.1) is expressed as: Find $u \in \mathcal{U}$ such that

$$a(w, u) + a(w, u)_{\Gamma_h} = (w, f) + (w, \bar{q})_{\Gamma_q} + (w, u_\infty)_{\Gamma_h}, \quad \forall w \in \mathcal{V}. \tag{2.2}$$

where the linear and bilinear forms in Equation (2.2) are

$$\begin{aligned}
 a(w, u) &= \int_{\Omega} \kappa \nabla w \cdot \nabla u \, d\Omega, \\
 a(w, u)_{\Gamma_h} &= \int_{\Gamma_h} h w u \, d\Gamma, \\
 (w, f) &= \int_{\Omega} w f \, d\Omega, \\
 (w, \bar{q})_{\Gamma_q} &= \int_{\Gamma_q} w \bar{q} \, d\Gamma, \\
 (w, u_{\infty})_{\Gamma_h} &= \int_{\Gamma_h} h w u_{\infty} \, d\Gamma.
 \end{aligned} \tag{2.3}$$

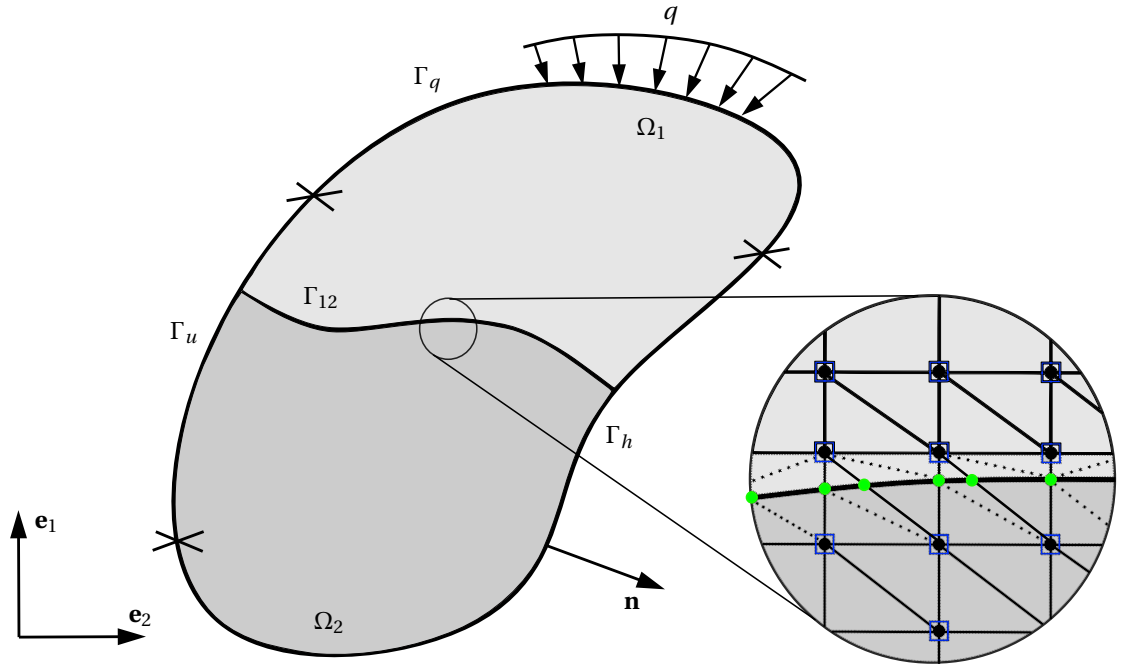


Figure 2.1: Schematic of domain Ω used in the formulation of the problem. The boundary of the domain is split into three distinct regions Γ_u , Γ_q and Γ_h , where Dirichlet, Neumann and Robin boundary conditions are prescribed. The domain is composed of two mutually exclusive material phases, Ω_1 and Ω_2 . The inset shows the discretization with a material interface that is non-matching to the mesh. Original mesh nodes are represented with black circles, enriched IGFEM nodes and GFEM DOFs are denoted as green circles and blue squares, respectively.

The Galerkin projection is applied to the weak form in Equation (2.2) to approximate the solution. For the Galerkin approximation, let $\mathcal{V}^h \subset \mathcal{V}$ and $\mathcal{U}^h \subset \mathcal{U}$ be finite-dimensional sets such that $\mathcal{V}^h = \{v^h : v^h|_{\Gamma_u} = 0\}$ and $\mathcal{U}^h = \{u^h : u^h = v^h + t^h, t^h|_{\Gamma_u} = \bar{u}\}$. Then the Galerkin form of the boundary value problem is

$$a(w^h, v^h) + a(w^h, v^h)_{\Gamma_h} = (w^h, f) + (w^h, \bar{q})_{\Gamma_q} + (w^h, u_{\infty})_{\Gamma_h} - a(w^h, t^h), \quad \forall w^h \in \mathcal{V}^h. \tag{2.4}$$

Equation (2.4) can be approximated using the Generalized Finite Element Method (GFEM) and the Interface-enriched Generalized Finite Element Method (IGFEM) by discretizing the domain with finite elements. One problem in GFEM framework is that the application of Dirichlet boundary condition is not straightforward, because of the non-zero enrichment functions at the nodes with prescribed temperature value. Thus, one must employ techniques such as the penalty method or Lagrange multipliers to enforce Dirichlet boundary

conditions [47, 48]. In this work, the penalty method is adopted due to the simplicity in its implementation. Then the Galerkin form becomes

$$a(w^h, u^h) + a(w^h, u^h)_{\Gamma_h} + \rho(w^h, u^h - \bar{u})_{\Gamma_u} = (w^h, f) + (w^h, \bar{q})_{\Gamma_q} + (w^h, u_\infty)_{\Gamma_h}, \quad \forall w^h \in \mathcal{V}^h. \quad (2.5)$$

where $\rho(w^h, u^h - \bar{u})_{\Gamma_u} = \rho \int_{\Gamma_u} w^h (u^h - \bar{u}) d\Gamma$ is the penalty method part term, ρ is the penalty parameter.

2.2. GFEM^{sd} Formulation

Considering the advantages of GFEM and IGFEM, we now solve the weak discontinuity heat transfer problem with high thermal gradients by employing the Generalized Finite Element Method with spread and discrete enrichments (GFEM^{sd}), which combines both IGFEM and GFEM formulations. The term ‘‘spread’’ refers to the GFEM enrichments applied over the discretized domain, and ‘‘discrete’’ means IGFEM enrichments locating at the material discontinuities. This GFEM^{sd} formulation has the temperature approximation form as

$$u^h(\mathbf{x}) = \underbrace{\sum_{i \in \iota_h} N_i(\mathbf{x}) \tilde{U}_i}_{\text{FEM}} + \underbrace{\sum_{i \in \iota_d} \psi_i(\mathbf{x}) \alpha_i}_{\text{IGFEM}} + \underbrace{\sum_{i \in \iota_h} N_i(\mathbf{x}) \sum_{j \in \iota_s} \varphi_{ij}(\mathbf{x}) \hat{U}_{ij}}_{\text{GFEM}} \quad (2.6)$$

Equation (2.6) has three terms with different functions. The first term is the standard Finite Element Method (FEM) approximation, $N_i(\mathbf{x})$ and \tilde{U}_i are the standard shape functions and degrees of freedom (DOFs), respectively. ι_h is an index corresponding to all the original nodes of the mesh. The second term is IGFEM approximation, $\psi_i(\mathbf{x})$ are IGFEM enrichment functions which are constructed by means of Lagrange shape functions of integration elements, α_i are IGFEM enriched DOFs associated with IGFEM enriched nodes which are created at the intersections of elements edges and material interfaces. ι_d is the index set of all the created IGFEM nodes. This second term enables GFEM^{sd} to capture weak discontinuities at material interfaces. The last term denotes GFEM approximation that serves to resolve the high thermal gradients. $\varphi_{ij}(\mathbf{x})$ are enrichment functions associated with GFEM enriched DOFs \hat{U}_{ij} . ι_s is the index set of GFEM enrichment functions. It should be noted that in GFEM^{sd} formulation, the GFEM enriched DOFs are added to all the background mesh nodes. As the heat conduction problems in this work exhibits high thermal gradients, GFEM enrichment functions should have strong nonlinear characteristics. Therefore, GFEM enrichment function used in this work is a scaled exponential function, $\varphi_{ij}(\mathbf{x}) = e^{\frac{-\mathbf{x}}{c}}$, where c is a scaling coefficient related to the domain size. An introduction of GFEM and IGFEM formulations can be found in Appendix A.

Starting from Equation (2.6), the discrete approximation of weak form Equation (2.5) can be expressed as

$$\mathbf{K}\mathbf{U} = \mathbf{F} \quad (2.7)$$

where \mathbf{K} and \mathbf{F} are the stiffness matrix and force vector, \mathbf{U} is the vector of DOFs, namely standard and enriched DOFs. In GFEM^{sd} formulation, enriched DOFs contain both IGFEM and GFEM DOFs. Then we derive \mathbf{K} and \mathbf{F} .

As illustrated in the inset of Figure 2.1, the model domain contains two materials with different heat conductivity κ_1 and κ_2 . The domain is meshed by triangle elements. Cut elements, *i.e.*, elements intersected by the material interfaces, are divided into cut sub-elements. Therefore, there are two kinds of elements in the domain: (a) Original mesh elements, which contain FEM DOFs and GFEM enriched DOFs. (b) Cut sub-elements, which contain all the FEM DOFs, IGFEM and GFEM enriched DOFs.

First, we look at the general element case, which refers to cut sub-elements. Let $\boldsymbol{\phi}$ be the matrix contains all the standard shape functions and enrichment functions on element e , and \mathbf{B} be the matrix of derivatives of these shape and enrichment functions

$$\boldsymbol{\phi} = [N_1 \quad \cdots \quad \psi_1 \quad \cdots \quad N_1\varphi_1 \quad \cdots], \quad (2.8)$$

$$\mathbf{B} = \begin{bmatrix} \frac{\partial N_1}{\partial x} & \dots & \frac{\partial \psi_1}{\partial x} & \dots & \frac{\partial (N_1 \varphi_1)}{\partial x} & \dots \\ \frac{\partial N_1}{\partial y} & \dots & \frac{\partial \psi_1}{\partial y} & \dots & \frac{\partial (N_1 \varphi_1)}{\partial y} & \dots \\ \frac{\partial N_1}{\partial z} & \dots & \frac{\partial \psi_1}{\partial z} & \dots & \frac{\partial (N_1 \varphi_1)}{\partial z} & \dots \end{bmatrix}. \quad (2.9)$$

Chain-rule [50] is adopted when calculating the derivatives in \mathbf{B} matrix. The element DOFs arrangement sequence in $\boldsymbol{\phi}$ and \mathbf{B} is the same: FEM DOFs, IGFEM enriched DOFs, and GFEM enriched DOFs.

Next, for the original mesh elements, we only need to remove the GFEM contribution part in $\boldsymbol{\phi}$ and \mathbf{B} to obtain new corresponding matrices.

Then, the stiffness matrix \mathbf{k}_e of this element is constructed as

$$\mathbf{k}_e = \mathbf{k}_{el} + \mathbf{k}_\rho + \mathbf{k}_h \quad (2.10)$$

where \mathbf{k}_{el} is the element local stiffness matrix related to material heat conductivity, \mathbf{k}_ρ is the penalty stiffness matrix along Dirichlet boundary and \mathbf{k}_h is the Robin boundary condition stiffness matrix.

And the element force vector \mathbf{f}_e is

$$\mathbf{f}_e = \mathbf{f}_{el} + \mathbf{f}_\rho + \mathbf{f}_h + \mathbf{f}_q \quad (2.11)$$

where \mathbf{f}_{el} is the element local force vector related to material heat conductivity, \mathbf{f}_ρ is the element Dirichlet boundary force vector, and \mathbf{f}_h and \mathbf{f}_q are force vectors for Robin and Neumann boundary conditions, respectively.

The expression for terms in Equations (2.10) and (2.11) are

$$\begin{aligned} \mathbf{k}_{el} &= \int_e \boldsymbol{\kappa}_i \mathbf{B}^\top \mathbf{B} \, de, \\ \mathbf{k}_\rho &= \rho \int_{\partial e} \boldsymbol{\phi}^\top \boldsymbol{\phi} \, d\partial e, \\ \mathbf{k}_h &= h \int_{\partial e} \boldsymbol{\phi}^\top \boldsymbol{\phi} \, d\partial e, \\ \mathbf{f}_{el} &= \int_e \boldsymbol{\phi}^\top f \, de, \\ \mathbf{f}_\rho &= \rho \int_{\partial e} \boldsymbol{\phi}^\top \bar{u} \, d\partial e, \\ \mathbf{f}_h &= h \int_{\partial e} \boldsymbol{\phi}^\top u_\infty \, d\partial e, \\ \mathbf{f}_q &= \int_{\partial e} \boldsymbol{\phi}^\top \bar{q} \, d\partial e. \end{aligned} \quad (2.12)$$

Then the discrete system of linear Equation (2.7) is obtained by FEM standard assembly procedure, except that enrichments are incorporated

$$\mathbf{K} = \mathbb{A} \mathbf{k}_e, \quad \mathbf{F} = \mathbb{A} \mathbf{f}_e. \quad (2.13)$$

where \mathbb{A} is the standard FEM assembly procedure operator.

The elements used in the following simulation work are three-node triangular (t3) element for 2D problem and four-node tetrahedron (T4) element for 3D problem. Gauss integration rules with three gauss points are used in integration elements.

2.3. Comparison of GFEM^{sd}, IGFEM and GFEM

Strengths and limitations of GFEM^{sd}, IGFEM and GFEM when tackling with high thermal gradients problem in composite are listed below.

- In GFEM, because enrichment functions are usually not zero at nodes, except for some special enrichments such as the Ridge enrichment introduced by Mões *et al.* [51], the prescribed nodal temperature values cannot be assigned directly. Thus, the imposition of Dirichlet boundary conditions is not straightforward. This problem still exists in GFEM^{sd}, therefore, the Dirichlet boundary condition needs penalty method to be prescribed weakly.
- About high thermal gradients, GFEM can capture the gradients by enriching the finite element space. But in IGFEM, the solution accuracy depends on FEM approximation, and mesh refinement could be implemented in regions where gradients are too steep. In GFEM^{sd}, GFEM enriched DOFs are added to all the background mesh nodes. As a consequence, there is no blending element issue [52], and the high thermal gradients can be well resolved by GFEM enrichments contribution.
- When encountering with material interfaces, in GFEM, enriched DOFs are attached to original mesh nodes near the weak discontinuities, and extra enrichments are applied to deal with the weak discontinuities [53]. GFEM enriched DOFs represent temperatures after interpolation. While in IGFEM, enriched DOFs are associated with new nodes created along the discontinuities and directly represent temperature solutions. GFEM^{sd} adopts the principle of IGFEM to add enriched DOFs to capture discontinuity temperature fields. In summary, GFEM and IGFEM methods play to their strengths in GFEM^{sd} formulation to solve the above-mentioned problem.

2.4. Numerical Examples

In the following sections, 2D and 3D heat conduction problems are presented. The 2D problems having exact solutions demonstrate the accuracy of GFEM^{sd} in addressing high thermal gradients in composite. In 2D problems, no units are specified; therefore, any consistent unit system can be assumed. In the 3D problem, a twill pattern composite material model is studied systematically, including the configuration of fiber geometry, the temperature distribution when subjected to high thermal gradients, and effective heat conductivity properties. Finally, a fiber shape optimization is conducted to achieve the minimum effective heat conductivity of the composite for a given constant fiber volume.

2.4.1. One-Dimensional Heat Source Conduction Problem

This example is used to verify the proposed GFEM^{sd} formulation and the spread exponential enrichment function in an equivalent 1D heat conduction problem. Let the temperature field over the domain $\Omega = 1 \times 1$ to be defined as (see Figure 2.2)

$$u(x, y) = \begin{cases} 2000(x - 0.5)e^{-x} + 1050 & 0 \leq x \leq 0.5, \\ 10000(x - 0.5)e^{-x} + 1050 & 0.5 < x \leq 1. \end{cases} \quad (2.14)$$

This manufactured temperature solution is constant in the y direction and uses an exponential function. The material interface locates at $x = 0.5$ and material heat conductivity coefficients are $\kappa_1 = 5$ and $\kappa_2 = 1$ to the left and right of the material interface, respectively. The body source term is then obtained by

$$f(x, y) = -\nabla \cdot (\boldsymbol{\kappa} \nabla u) = -(10000x - 25000)e^{-x}. \quad (2.15)$$

Top and bottom edges are insulated (heat flux $\bar{q} = 0$), and temperature values $\bar{u} = 50$ and $\bar{u} = 2889.4$ are prescribed to the left and right edges, respectively. The Dirichlet boundary conditions are enforced weakly by means of penalty method. For the numerical solution, GFEM^{sd} with spread exponential enrichment function is used to get an approximation of the temperature field. Figure 2.3 compares the numerical to the analytical result, showing that GFEM^{sd} is capable of capturing the temperature field accurately.

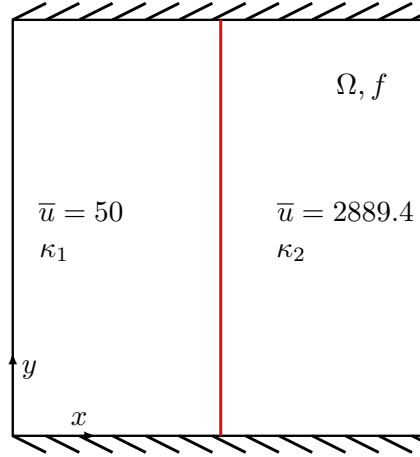


Figure 2.2: Schematic for two different materials of 1D heat source conduction problem. Material interface locates at $x = 0.5$. Boundary conditions include prescribed temperatures \bar{u} at left and right edges, insulated bottom and top edges.

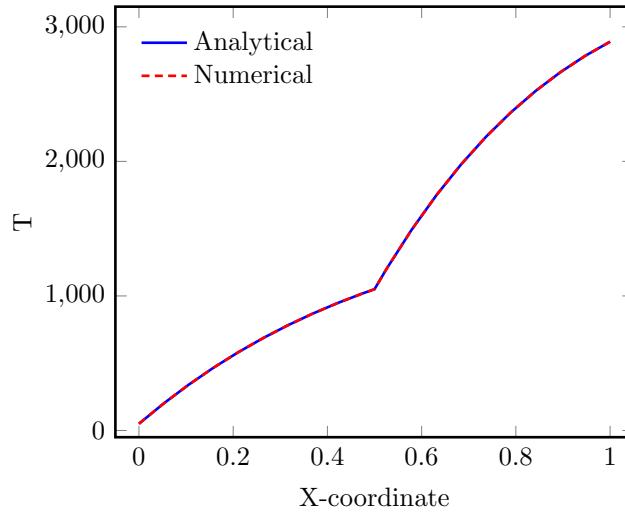


Figure 2.3: Temperature field of 1D heat source conduction problem.

To investigate the convergence and accuracy of GFEM^{sd}, the L^2 norm and the energy norm of the error are used, which are defined as

$$\|u - u^h\|_{L^2(\Omega)} = \sqrt{\int_{\Omega} (u - u^h)^2 d\Omega} \quad (2.16)$$

$$\|u - u^h\|_{E(\Omega)} = \sqrt{\int_{\Omega} (u - u^h)^2 d\Omega + \int_{\Omega} (\nabla u - \nabla u^h)^2 d\Omega} \quad (2.17)$$

Figures 2.4 and 2.5 summarizes the results of the convergence study, where GFEM^{sd} is compared to an IGFEM reference solution without spread exponential enrichment. Figure 2.4(a) shows the L^2 norm of the error as a function of the number of DOFs while Figure 2.4(b) is L^2 norm with the mesh size. As observed in these figures, GFEM^{sd} yields faster convergence rates than IGFEM which is 1.997 with respect to mesh size. Moreover, since the spread enrichment has a similar form as the exact solution in this example, L^2 norm error is greatly reduced in GFEM^{sd} as compared to IGFEM, which demonstrates the strength of GFEM^{sd} in coping with high gradients problem. Similar phenomena can also be observed in the energy norm results, and GFEM^{sd} performs better than IGFEM as shown in Figure 2.5.

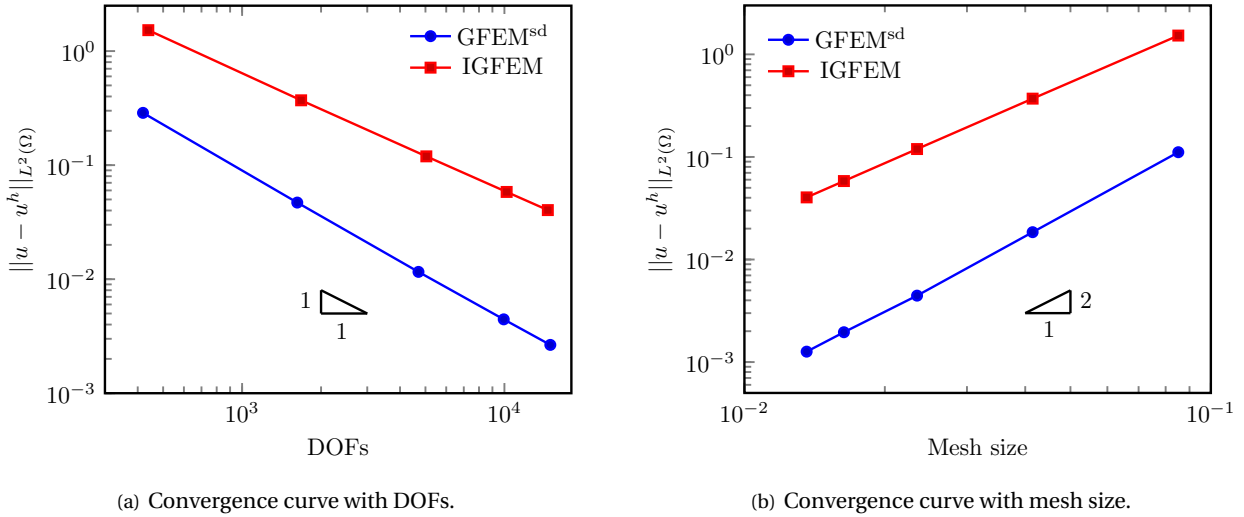


Figure 2.4: Convergence results in L^2 norm of the error with respect to (a) the total number of DOFs and (b) mesh size of the 1D heat source conduction problem.

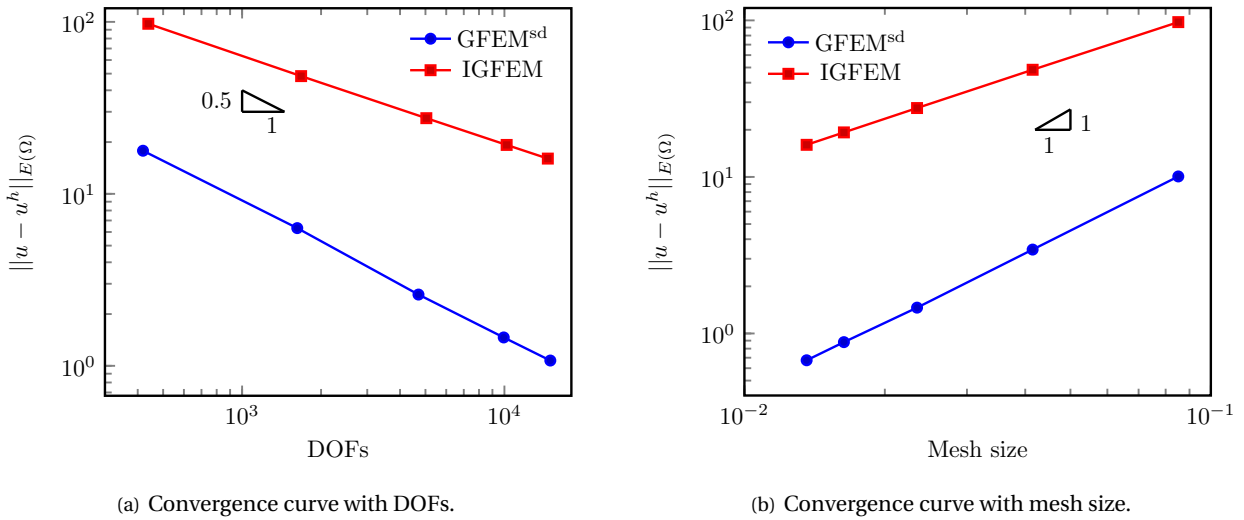


Figure 2.5: Convergence results in energy norm of the error with respect to (a) the total number of DOFs and (b) mesh size of the 1D heat source conduction problem.

2.4.2. Two-Dimensional Source Heat Conduction Problem

After testing GFEM^{sd} in a 1D heat source problem, we now turn to a 2D heat conduction problem, where we spatially vary the heat source along two directions. Let the domain be the same as in the first example and let the exact temperature field be

$$u(x, y) = \begin{cases} 100 \times \cos(3\pi x) \cos(3\pi y) + 550 & 0 \leq x \leq 0.5, \\ 500 \times \cos(3\pi x) \cos(3\pi y) + 550 & 0.5 < x \leq 1. \end{cases} \quad (2.18)$$

Then the body source is

$$f(x, y) = 9000 \times \pi^2 \cos(3\pi x) \cos(3\pi y) \quad (2.19)$$

The material heat conductivity coefficients and material interface location are the same as the previous 1D example. The Dirichlet boundary conditions with spatially changing values are applied to all the edges, which

are

$$u_{\text{left}} = 100 \times \cos(3\pi y) + 550, \quad u_{\text{right}} = 550 - 500 \times \cos(3\pi y). \quad (2.20)$$

$$u_{\text{top}} = \begin{cases} -100 \times \cos(3\pi x) + 550 & 0 \leq x \leq 0.5, \\ -500 \times \cos(3\pi x) + 550 & 0.5 < x \leq 1, \end{cases}, \quad u_{\text{bottom}} = \begin{cases} 100 \times \cos(3\pi x) + 550 & 0 \leq x \leq 0.5, \\ 500 \times \cos(3\pi x) + 550 & 0.5 < x \leq 1, \end{cases}. \quad (2.21)$$

The temperature field simulation result is illustrated in Figure 2.6. To better compare the numerical and analytical solutions, a typical temperature solution along the straight line $y = 0.3$ is plotted in Figure 2.7. The result shows that GFEM^{sd} can also obtain an accurate numerical solution in this 2D example.

The convergence results for this example are shown in Figures 2.8 and 2.9. GFEM^{sd} is also more accurate than IGFEM, showing that GFEM^{sd} can solve high thermal gradients problems accurately even without a similar spread enrichment as the exact solution. Besides, GFEM^{sd} recovers the convergence rate of 1.9749 in L^2 norm error with respect to mesh size which is almost the same as IGFEM.

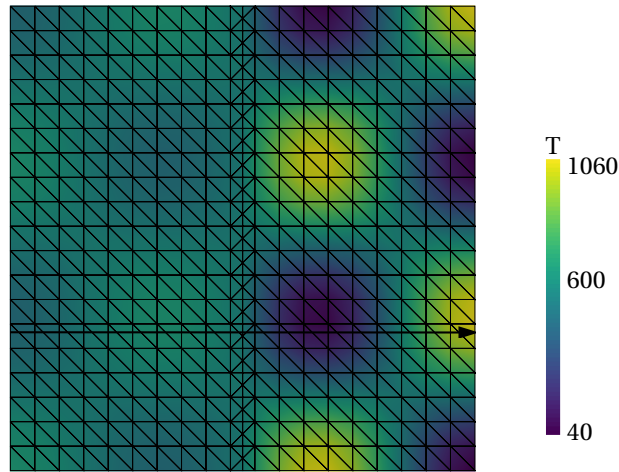


Figure 2.6: Temperature field of 2D heat source conduction problem.

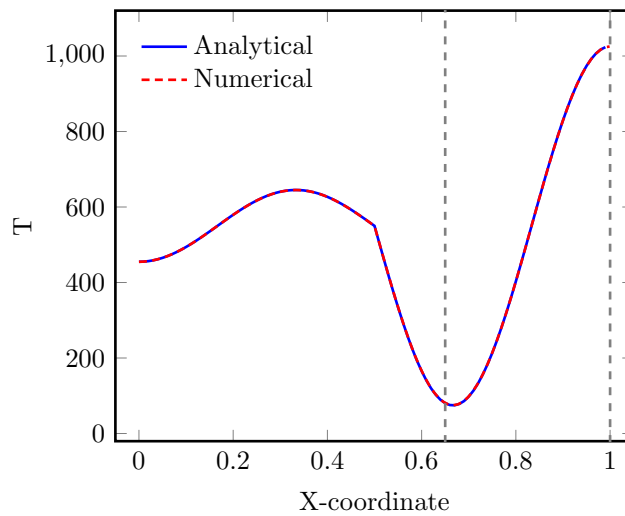


Figure 2.7: Temperature field along the black arrow in Figure 2.6 of 2D heat source conduction problem. The high gradients locate approximately between the two dashed gray lines.

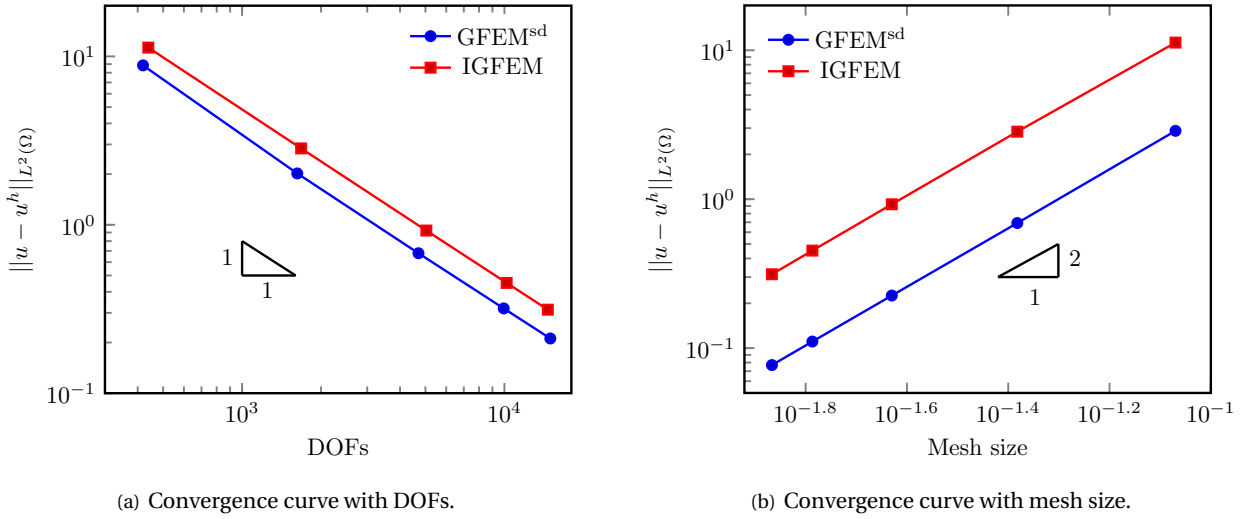


Figure 2.8: Convergence results in L_2 norm of the error with respect to (a) the total number of DOFs and (b) mesh size of the 2D heat source conduction problem.

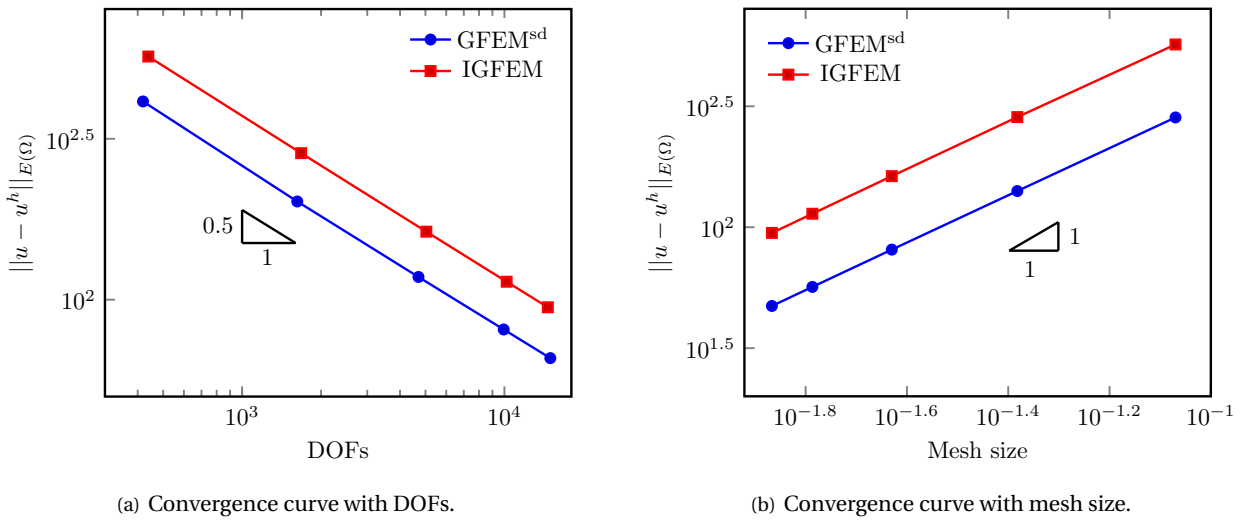


Figure 2.9: Convergence results in energy norm of the error with respect to (a) the total number of DOFs and (b) mesh size of the 2D heat source conduction problem.

2.4.3. Multiple Curved Material Interfaces

This example is using GFEM^{sd} to analyze 2D heat conduction problem with multiple curved material interfaces. The effect of material mismatch, which is the material heat conductivity coefficients difference across material interface, on the performance of GFEM^{sd} is studied as well.

The domain $\Omega = 4 \times 4$ is discretized with a $20 \times 20 \times 2$ triangle elements. The two material interfaces are described by cosine functions with an offset shown as

$$\begin{cases} i_1(x, y) = \cos\left(\frac{1}{2}\pi x\right) + 2.3, \\ i_2(x, y) = \cos\left(\frac{1}{2}\pi x\right) + 1.7. \end{cases} \quad (2.22)$$

The mismatch of heat conductivity between the two material interfaces causes the weak discontinuity. The domain, boundary conditions and material phases are shown in Figure 2.10(a). A constant heat flux $\bar{q} = 100$

is applied to the top edge, and the bottom edge has a prescribed Robin boundary condition with ambient temperature $u_\infty = 15$ and heat transfer coefficient $h = 7.9$. Left and right edges are insulated. The material mismatch are investigated corresponding to three values of the thermal conductivity ratio $\beta = \kappa_2/\kappa_1 = 5, 50,$ and 100 with $\kappa_1 = 1$. The spread enrichment function is adopted as $\varphi = e^{-\frac{y}{c}}$ because the heat flux is applied in the y direction.

The temperature fields obtained with GFEM^{sd} are presented in Figure 2.10(b), 2.10(c) and 2.10(d), separately. Figure 2.11 gives the temperature field along the line $x = 2$ in the domain. These figures show that GFEM^{sd} can capture the temperature field smoothly with increasing gradient discontinuity across material interfaces.

Because the exact solution for this problem is not available, so convergence rates will be measured with respect to the energy norm error where the exact strain energy is obtained using *a posteriori* estimate. The relative error e_r is computed as

$$e_r = \|u^p - u^h\|_{E(\Omega)} = \sqrt{a(u^p, u^p) - a(u^h, u^h)} \tag{2.23}$$

where u^p is *a posteriori* estimate of the exact solution.

The convergence results are in Figure 2.12, showing that GFEM^{sd} stills performs better than IGfEM for all the three material mismatch cases when the mesh sizes are predefined.

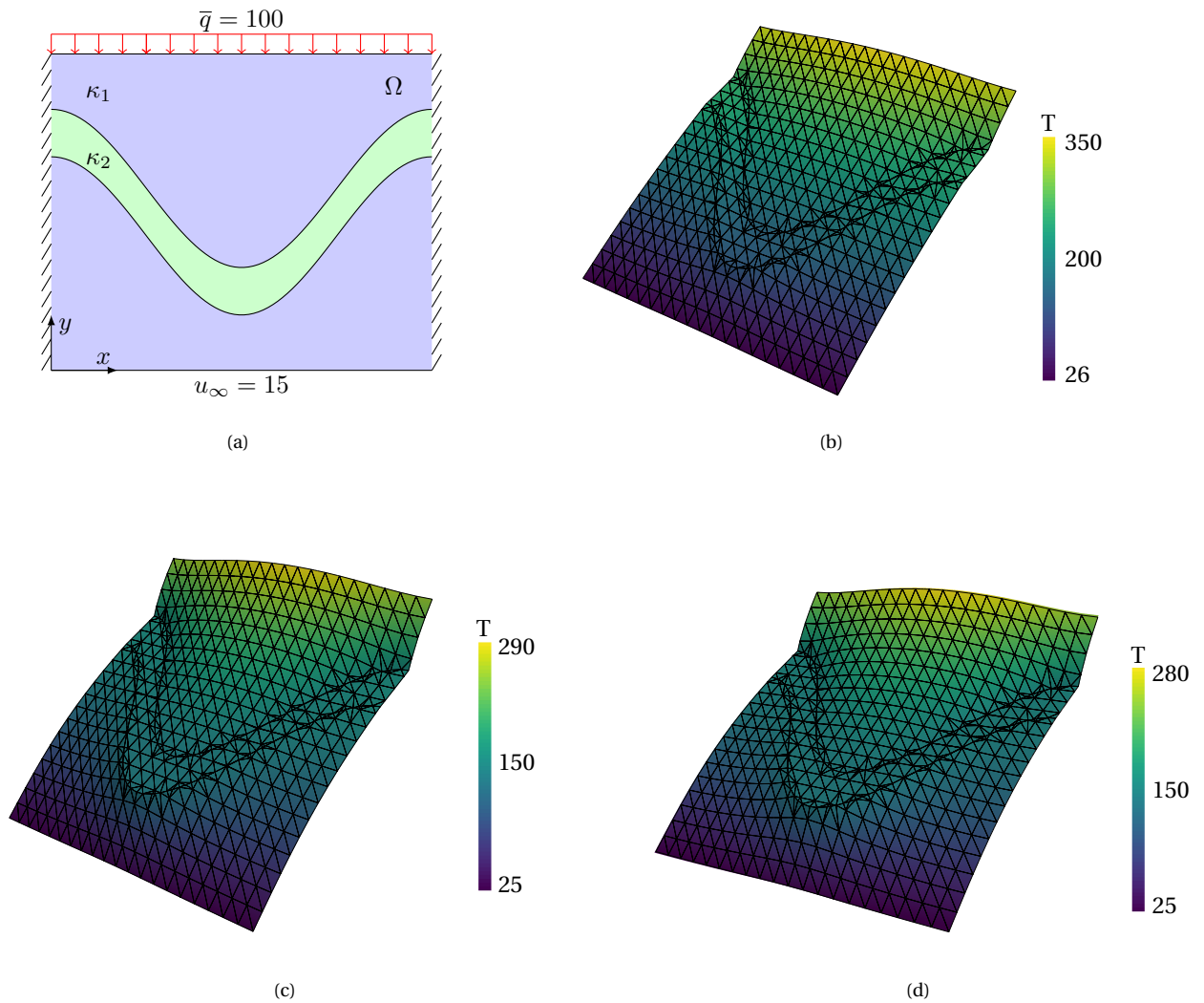


Figure 2.10: (a) Schematic of domain geometry and boundary conditions of the multiple curved material interfaces example, temperature field for (b) $\kappa_2/\kappa_1 = 5$, (c) $\kappa_2/\kappa_1 = 50$, (d) $\kappa_2/\kappa_1 = 100$ with $\kappa_1 = 1$.

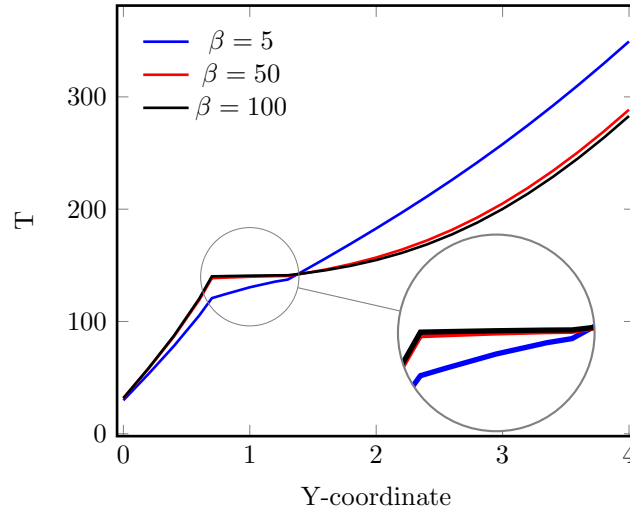


Figure 2.11: Temperature fields along the line $x = 2$ of multiple curved material interfaces problem.

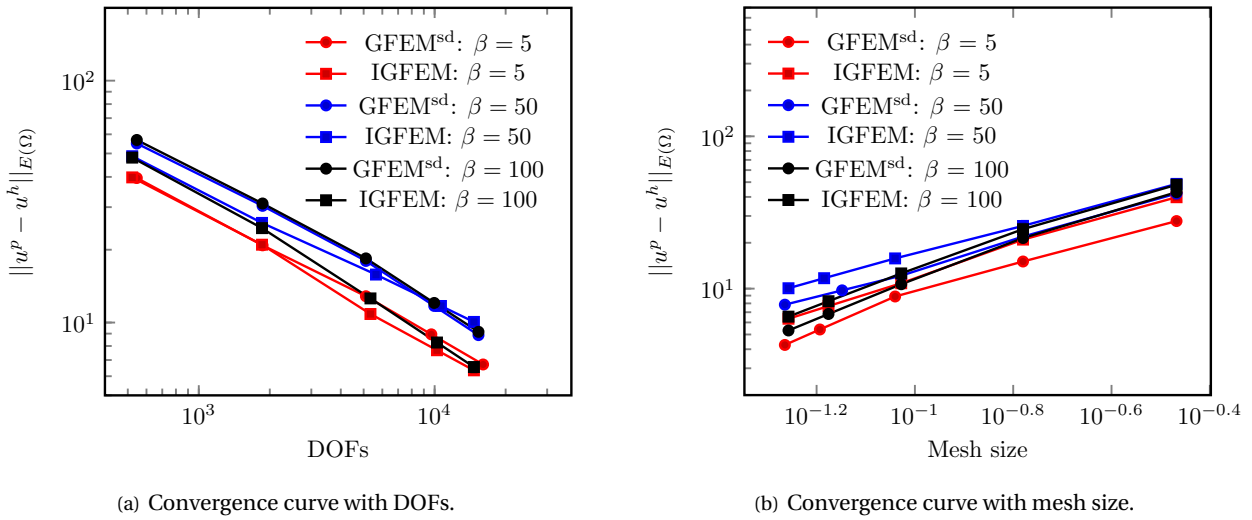


Figure 2.12: Convergence results in energy norm of the error with respect to (a) the total number of DOFs and (b) mesh size of the multiple curved material interfaces problem.

2.5. Three-Dimensional Twill Pattern Composite

In the above 2D numerical examples, we demonstrated the accuracy of GFEM^{sd} in addressing high thermal gradients problems with material discontinuities. In this section, we focus on the 3D twill pattern composite, studying the temperature distribution, the effective heat conductivity coefficients, and the fiber shape optimization.

2.5.1. Three-Dimensional Twill Pattern Composite Geometric Modelling

Twill pattern composites consist of longitudinal and transverse fibers in a pattern of over two and under two repetition as shown in Figure 2.13. As the weaving pattern can be defined by a basic repeating unit, it is commonly to use the repetitive unit cell to construct a representative volume element (RVE) for analyzing the composite's behavior. Figure 2.14 illustrates the twill composite idealized RVE model.



Figure 2.13: A twill weave fabric of the twill pattern composite.

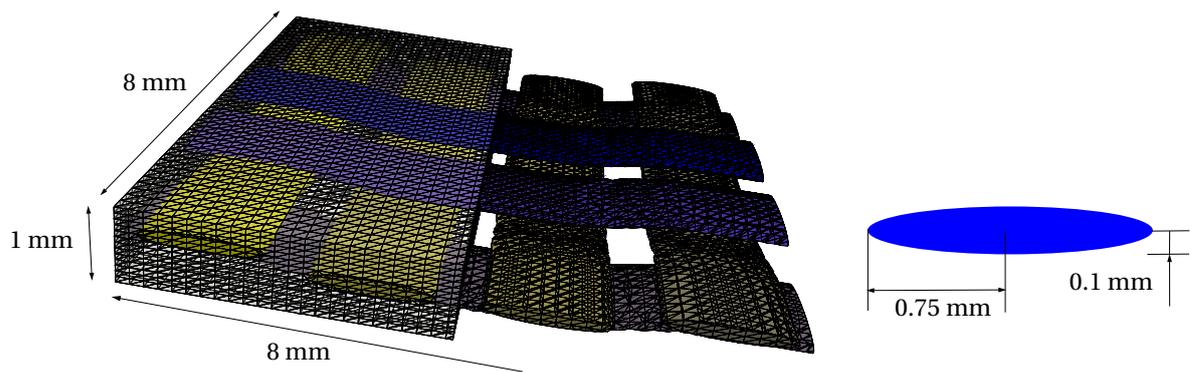


Figure 2.14: The idealized RVE model of twill pattern composite, structured mesh of the background, conforming mesh of the twill pattern fibers, and the cross-section of fibers.

We assume that there is no space between the fiber bundles in the RVE model. The cross-section shape of each fiber is modelled as an ellipse with semi-major axis $r = 0.75\text{ mm}$ and semi-minor axis $b = 0.1\text{ mm}$. The centerline of fiber can be split into seven segments, each segment has its mathematical function to describe its position, see Appendix B for the mathematical equations of the fiber's centerline position. Eight fibers are immersed in the matrix to form the RVE model. The RVE model has a dimension size $8 \times 8 \times 1\text{ mm}$, see in Figure 2.14. The fiber and matrix heat conductivity coefficients κ_f, κ_m are $10\text{ W}/(\text{m} \cdot \text{K})$ and $65\text{ W}/(\text{m} \cdot \text{K})$, respectively.

In the modelling process, a level set function [57, 58] is used to describe the boundary of the fibers. Then, a Neumann boundary condition with uniform heat flux $\bar{q} = 10\text{ W}/\text{m}$ and Dirichlet boundary condition $\bar{u} = 50\text{ K}$ are prescribed to the top and bottom surfaces of the model, respectively. The other model surfaces are considered as insulated. Figure 2.15 illustrates the temperature field of this twill composite model. It can be seen that the temperature field is symmetric which conforms to the symmetry of the structure of the RVE model.

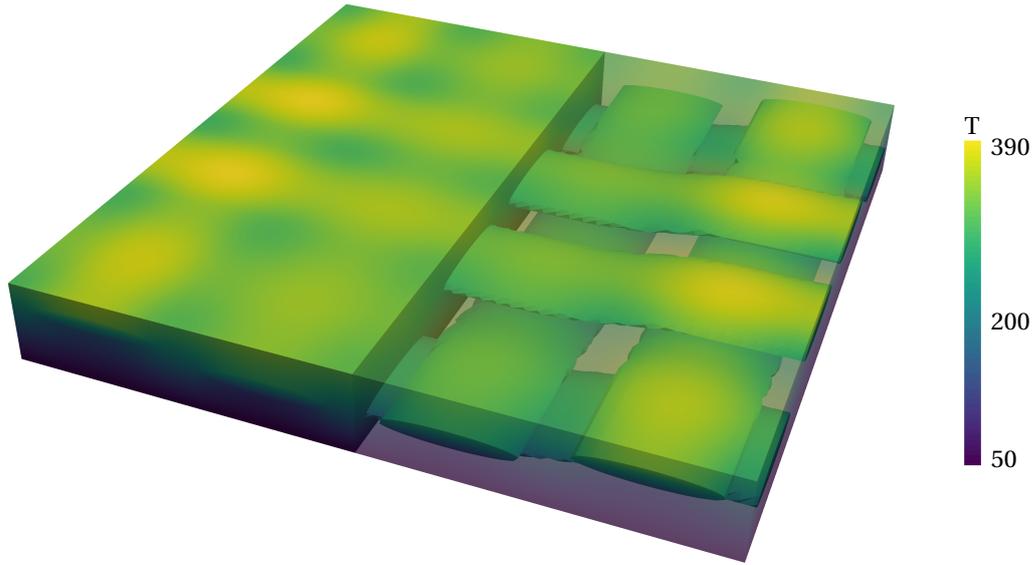


Figure 2.15: Temperature distribution of the twill RVE model.

2.5.2. Effective Heat Conductivity and Boundary Conditions of the RVE Model

In this work, the composite properties are orthotropic. The effective heat conductivity coefficients are κ_{ex} , κ_{ey} and κ_{ez} , then we relate the composite's heat flux to temperature gradients as

$$\begin{bmatrix} \bar{q}_x \\ \bar{q}_y \\ \bar{q}_z \end{bmatrix} = \begin{bmatrix} \kappa_{ex} & 0 & 0 \\ 0 & \kappa_{ey} & 0 \\ 0 & 0 & \kappa_{ez} \end{bmatrix} \begin{bmatrix} \frac{\partial u}{\partial x} \\ \frac{\partial u}{\partial y} \\ \frac{\partial u}{\partial z} \end{bmatrix}. \quad (2.24)$$

We determine the main effective heat conductivity coefficients as follows: For a 3D composite RVE model, considering the surface with area A through which heat flux \bar{q} passes, the component of heat conduction equation along z direction can be described as

$$\Phi = - \int \kappa_{ez} \frac{\partial u}{\partial z} dA, \quad (2.25)$$

where Φ is the heat difference between the two surfaces in z direction.

When calculating the effective heat conductivity along the z direction, Dirichlet and Neumann boundary conditions are prescribed on surfaces, $z = 0$ and $z = l$, respectively, while other surfaces are insulated. These boundary conditions are

$$\begin{cases} \bar{q}|_{z=l} = -\kappa_{ez} \frac{\partial u}{\partial z} \cdot \mathbf{n}, \\ u|_{z=0} = u_1. \end{cases} \quad (2.26)$$

With these boundary conditions, the heat flux \bar{q} is constant, so the heat gradient $\kappa_{ez} \frac{\partial u}{\partial z}$ is constant, then Equation (2.25) can be rewritten as

$$\Phi = -\kappa_{ez} \frac{\partial u}{\partial z} A. \quad (2.27)$$

Considering the temperature u_1 and u_2 on the two surfaces and length l between the surfaces, Equation (2.27) can be rearranged as the following term

$$\kappa_{ez} = -\frac{\Phi}{A} \cdot \frac{\partial z}{\partial u} = -\frac{\Phi}{A} \cdot \frac{l}{u_2 - u_1} = -\bar{q} \cdot \frac{l}{u_2 - u_1}, \quad (2.28)$$

where the temperature u_1 on Dirichlet boundary condition surface is set in advance, the temperature u_2 on Neumann boundary condition surface temperature can be determined by the surface average temperature evaluated from GFEM^{sd} approximation, that is

$$u_2 = \frac{\sum_{i=1}^n u_{2,i} \cdot a_i}{\sum_{i=1}^n a_i} \quad (2.29)$$

where $u_{2,i}$ is the average temperature of each element on the Neumann boundary surface. In meshing process, the boundary surfaces are meshed by standard three-node triangle element. For each triangle element, $u_{2,i} = \frac{u_{e1} + u_{e2} + u_{e3}}{3}$, where u_{e1} , u_{e2} and u_{e3} are the nodal temperature in the element, n is total number of elements on the surface and a_i is the area of each element.

In such a way, the effective heat conductivity of RVE in z direction is determined by Equations (2.28) and (2.29). The same principle also applies to obtain the effective heat conductivity in x and y directions. A simple numerical test of the correctness of this method can be found in Appendix C. The effects of arbitrary internal fiber shape on the effective heat conductivity will be reflected on a macro scale. Predicting effective heat conductivity under other boundary conditions can be found in [59].

Figure 2.16 shows that the RVE effective heat conductivity as a function of the total DOFs. It can be seen that the obtained effective heat conductivities slightly change with DOFs. The values are more accurate with more DOFs for finer meshes are generated. Furthermore, κ_{ex} value is almost equal to that of κ_{ey} , this conforms to the symmetry of the structure of the RVE model. The value κ_{ez} is smaller than the other two values, for less matrix material volume fraction in z direction.

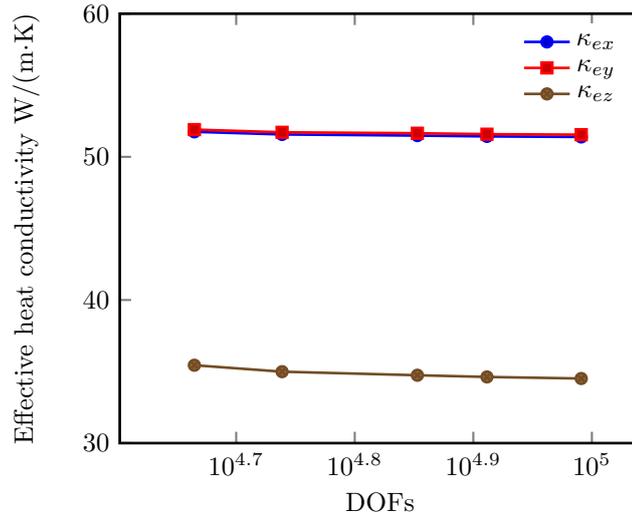


Figure 2.16: Three main effective thermal conductivity coefficients of the RVE model with respective to the number of DOFs.

2.5.3. Fiber Shape Optimization of the RVE Model

In this section, the effect of fiber parameters on the effective heat conductivity κ_{ez} is analyzed and GFEM^{sd} solver is combined with a gradient-based optimization scheme to optimize the shape of the embedded fibers in the RVE model.

Firstly, the fiber geometry is parameterized to easy the study. The fiber centerline vertical position z adopts a simple cosine function

$$z(x) = a \cos\left(\frac{2\pi x}{l_f}\right) \quad (2.30)$$

where a and l_f are the amplitude and wavelength of the fiber, x is the fiber horizontal location. In this way, the parameterized RVE model still keeps a similar fiber architecture as the twill pattern.

Because fiber has smaller heat conductivity value, the composite model will have smaller effective heat conductivity with more fiber, which can be speculated obviously based on the basic composite property Voigt model [60]. However, more fiber usually means a high manufacturing cost. To identify the best performance and cost-effective design, a fiber shape parameters design optimization scheme is conducted. The goal of the optimization work is to minimize the effective heat conductivity κ_{ez} under a fixed volume of fiber, which can be achieved by tailoring the fiber shape parameters a and b . The optimization problem consequently takes the form

$$\begin{aligned} \mathbf{s} : [a, b] = \underset{a, b}{\operatorname{argmin}} \quad & \kappa_{ez}, \\ \text{Subject to:} \quad & V_f = V_0, \\ & a \in [0.5, 1], \\ & b \in [0.5, 0.75]. \end{aligned} \quad (2.31)$$

where \mathbf{s} is the design variable vector and V_0 is the predefined fiber volume. With this objective function and constraints, the classic Sequential Quadratic Programming optimization algorithm [61] is adopted to solve this problem and a finite difference is used to get the partial derivative of the fiber volume $\frac{\partial V_f}{\partial a}$ and $\frac{\partial V_f}{\partial b}$.

Two different initial guess points are used to verify the optimization process efficiency. Their results are listed in Table 2.1. As shown in Table 2.1, the two initial designs converge to the same optimal design. Figure 2.17 gives an example of the iteration history and also the convergence curve.

Table 2.1: Optimal designs of the RVE geometry parameters

Design point	a	b	a/b	κ_{ez}
Initial 1	0.9309	0.5251	1.7728	46.9077
Optimal 1	0.6773	0.5522	1.2265	45.9947
Initial 2	0.6798	0.552	1.2315	46.0577
Optimal 2	0.6774	0.5522	1.2265	45.9947

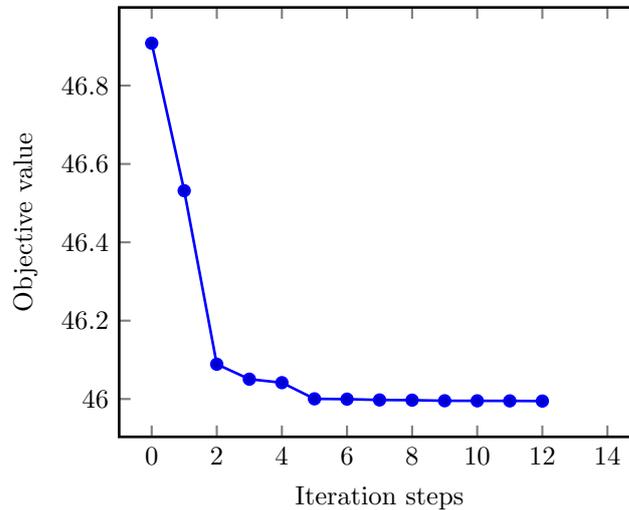


Figure 2.17: Optimization process convergence history.

To further research whether the optimum design in Table 2.1 is a global or local optimum, the relationship between objective function and the ratio a/b is roughly plotted in Figure 2.18. This curve is not strictly convex for the beginning local minimum. The previous two initial design points in Table 2.1 locate at the valley-shape domain such that converge to the global optimal design. When another initial point, for example, $\mathbf{s}_a = [0.54, 0.5679]$ with ratio $a/b = 0.9560$ is tested, the optimization process is stopped at the left-most point

in Figure 2.18. This phenomenon shows that the final optimal design of this objective function depends on the initial design point.

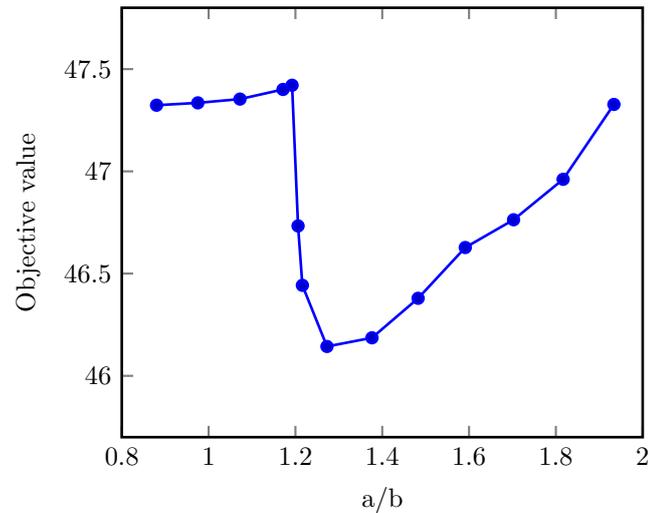


Figure 2.18: Objective function value with design variables ratio a/b .

With regards to finding the global optimal with an arbitrarily given initial design point, the Simulated Annealing algorithm [62] or other global optimization algorithm may provide a solution.

2.6. Conclusion

In this thesis, a new GFEM^{sd} formulation and its implementation for solving high thermal gradients in composites are presented. The feature of GFEM^{sd} is that by combing the formulations of GFEM and IGFEM, enriched DOFs are added to both the original mesh nodes and the interface nodes. This variation in the formulation of GFEM^{sd} eliminates mesh refinement issue when dealing with material discontinuity problems showing high thermal gradients. It was shown that GFEM^{sd} achieves more accurate solutions with less computational cost than IGFEM. Moreover, this method can capture the temperature gradient smoothly as the ratio of the material mismatch across material interfaces increases. We also investigate the application of GFEM^{sd} for 3D twill pattern composite. The geometric configuration of twill composite is well resolved by using a level set function, which parameterizes modelling of twill composite geometry. Based on effective heat conductivity of the composite model, fiber shape optimization is conducted to find the minimum effective heat conductivity subject to a given constant fiber volume. The results indicate that GFEM^{sd} solver can provide optimized designs in terms of enhanced thermal performance.

3

Reflection

3.1. Choice of Research Project

When choosing the research project for my master's thesis, I was intrigued by the interdisciplinary project "Computational Modelling of the Next Moon-Landing Composite Material". The service environment on the moon is severe, so components of moon-going equipment need to withstand high temperature and experience high thermal gradients. Composites are often used in this field of work because of their excellent material properties. Furthermore, composites are also utilized in maritime engineering and civil engineering, *etc.* Results from this project are thus widely applicable, versatile, and can be used to solve various engineering problems.

3.2. Process of The Project

The main challenges of the project were: (i) how to tackle with material weak discontinuities in composite, (ii) how to capture high thermal gradients accurately. To solve these problems, I proposed a New Generalized Finite Element Method with spread and discrete enrichments (GFEM^{sd}) to address high thermal gradients in composites. Also, a fiber shape optimization scheme is conducted to achieve the best balance between work performance and cost-effectiveness balance of the 3D twill composite. To complete this thesis project, I finished the following tasks:

- **Literature survey:** The first step was to perform an extensive survey of literature related to the project, which aimed to identify a "research gap". Literature about heat conduction problems, high gradients and composites was studied. Based on the literature survey, I proposed GFEM^{sd}, which combines both Generalized Finite Element Method and Interface-enriched Generalized Finite Element Method formulations to solve high thermal gradients in composites. This stage took me about three months.
- **Hybrida implementation:** The next step was implementing GFEM^{sd} formulation in *Hybrida* which is an in-house Python-based finite element library. It was challenging for me to start coding in *Hybrida* because *Hybrida* is an open library and all the group members can work on it, leading to a relatively messy code style in it. Several weeks were spent in getting familiar with *Hybrida*. After this, I started to write GFEM^{sd} formulation codes, including dofs-manager, boundary conditions, and post-processing, *etc.* I then verified the codes with an equivalent 1D heat conduction problem with an exact solution. The verification took me even longer time than writing codes. The carelessness I had which wrote codes paid for the price. Fortunately, by taking the advice of my supervisor and help of group members, I finally found the bugs in codes and got the right result. Later, 2D heat conduction problems were also verified to test the applicability of GFEM^{sd}.
- **3D twill composite problem:** Having verified the accuracy of GFEM^{sd} in 2D problems, then I moved to simulate the heat conduction problem in practical composite structure. I contacted Rahul Sharma who is also the project supervisor from the company ARCEON, showing my project progress to him. Rahul gave me 3D CAD drawings of their twill pattern composite, and I began to do the heat simulations. Because of the complex morphology of fibers in twill composite, it was really difficult to establish the geometric model and conduct the meshing process. The first try was to use 3D modelling software to create the fibers' architec-

ture directly, and then created the required mesh by immersed meshing in *Hybrida*. However, this was not working due to the parallel element edges of the fiber surface mesh and background mesh. Later, I found that using a levelset function to define the shape of fibers was an efficient way to create geometric models. This method also enabled me to change fiber geometric parameter easily. Next, I simulated the 3D twill composite heat conduction problem in a Representative Volume Element (RVE) model and got desirable results. Then, to better understand the macro thermal property of twill composite, the effective heat conductivity of RVE model was derived. Finally, I conducted a fiber shape optimization aiming to maximize thermal performance of twill composite.

While finishing these three tasks, I made steady progress towards my thesis project. During my thesis project I got valuable advice and help from my supervisor and group members when I was confronted with difficulties. Figure 3.1 shows the final timeline for my thesis project.

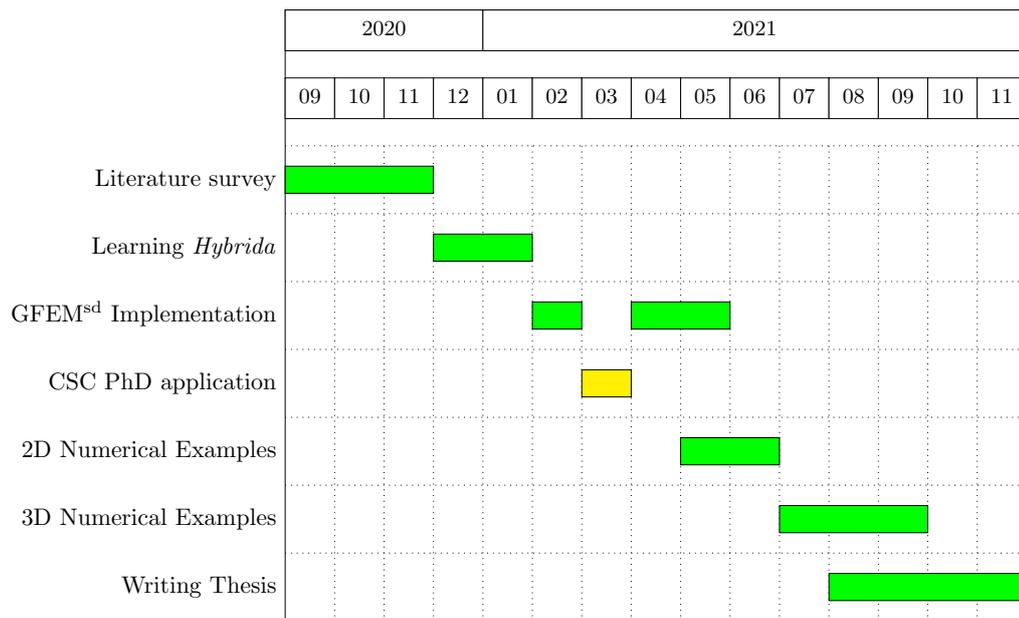


Figure 3.1: Final timeline for the thesis project.

3.3. Personal Improvement during The Project

The experience of working on thesis project was specious for me. From choosing the project to writing my thesis report, I have learned a lot during the process. Due to the influence of COVID-19, most of the time I was studying in my room, and I needed to overcome the loneliness and avoid slacking off. To complete the project as planned, I had to be self-motivated, which turned out to be very important. This also taught me useful time management skills. Always being to finish tasks as early as possible and never underestimate your work, because you will run into unexpected difficulties and challenges that you cannot plan for when you try to solve some problems. Setting aside time for these is a wise choice.

Besides these, I also obtained some professional skills. The Python coding experience which will be very useful for my the later study and work. Furthermore, the problem finding, searching of applicable methods, and problem-solving methods I learned were instrumental in helping me cultivate good thinking habits.

3.4. Future Work Prospections

Looking back at my thesis work, there are some aspects that can be further researched. The spread enrichments in current GFEM^{sd} work may not be the most suitable one, and better enrichments need to be found. In the optimization of 3D twill composite fiber shape, I used only two design variables; however more variables can be added, like fiber orientation angles. In addition, more efficient global optimization algorithm and topology optimization scheme could also be used in future applications of GFEM^{sd} to solve twill composite optimization problems.



Enriched Finite Element Methods

Enriched Finite Element Methods, such as Generalized Finite Element Method (GFEM) and Interface-enriched Generalized Finite Element Method (IGFEM) can be used for solving the high thermal gradients heat transfer problem in composite. Here, we present the formulations of the GFEM and IGFEM as the supplements for GFEM^{sd} method.

A.1. Generalized Finite Element Method

In GFEM computations, the domain is usually discretized by a finite element mesh that in general does not conform to the geometry of material interfaces, *i.e.*, geometry non-conforming mesh. In contrast to Finite Element Method (FEM), which usually uses mesh refinement to capture high thermal gradients, GFEM solves this problem by enriching the solution space near material interfaces and high thermal gradients region to add the missing solution information in FEM. In GFEM, this is done by choosing a set of enrichment functions $\{\varphi_{ij}(\mathbf{x}) : \mathbf{x} \rightarrow \mathbb{R} | N_i(\mathbf{x}) \neq 0\}_{j=1}^{n_{enr}}$, where n_{enr} is the number of enrichment function associated with node i . Then, a temperature approximation using GFEM takes the form

$$u^h(\mathbf{x}) = \underbrace{\sum_{i=1}^n N_i(\mathbf{x}) \tilde{u}_i}_{\text{FEM}} + \underbrace{\sum_{i=1}^n N_i(\mathbf{x}) \sum_{j=1}^{n_{enr}} \varphi_{ij}(\mathbf{x}) \hat{u}_{ij}}_{\text{GFEM}} \quad (\text{A.1})$$

where the first term is the standard FEM approximation and the second term is the GFEM contribution to the solution field. N_i is the standard FEM shape function, \tilde{u}_i and \hat{u}_{ij} are the standard and enriched DOFs, respectively. It should be noted that, now \tilde{u}_i at node i does not represent the field solution value, losing its original physical meaning based on Equation (A.1). The value of temperature at node i is then obtained as $u_i = \tilde{u}_i + \sum_{j=1}^{n_{enr}} \varphi_{ij}(\mathbf{x}) \hat{u}_{ij}$ due to the existence of enriched DOFs. A detailed description of GFEM can be found in reference [49].

A.2. Interface-enriched Generalized Finite Element Method

IGFEM, proposed by Soghrati *et al.* [29] was derived for problems containing weak discontinuities. In this method, the discretized background meshes are also non-conforming in the domain, but the cut elements, *i.e.*, elements cut by the material interfaces, are divided into small conforming sub-elements along the interfaces. At the intersection of element edges and material interfaces, enriched nodes are created and associated with enriched DOFs α_i , they serve to resolve the kinematics of a weak discontinuity. A temperature approximation through IGFEM has the form

$$u^h(\mathbf{x}) = \underbrace{\sum_{i=1}^n N_i(\mathbf{x}) \tilde{u}_i}_{\text{FEM}} + \underbrace{\sum_{i=1}^{n_{enr}} \psi_i(\mathbf{x}) \alpha_i}_{\text{IGFEM}} \quad (\text{A.2})$$

where $\psi_i(x)$ is the IGFEM enrichment function, that is constructed by means of Lagrange shape functions of integration elements. In this formulation, the node value \tilde{u}_i and α_i maintain their original physical meanings

A

in the field solution. The reader can refer to reference [29] for a more detailed description of IGFEM.

B

Mathematical Equation of The Twill Composite Fiber Centerline

To clarify the centerline position of the twill composite fiber, let us take the blue fiber in Figure B.1 as an example. The red dashed line is the fiber centerline and split into seven segments as shown in Figure B.2. The centerline locates in x - y plane, the left-most point's coordinate is defined as $(0,0.1)$, then l_1 to l_7 segment centerline coordinates are defined based on this point's coordinate.

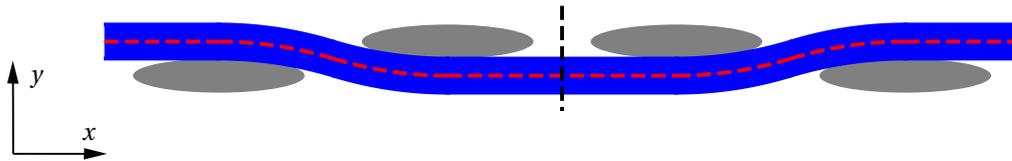


Figure B.1: Schematic of the fibers projection defined in 2D x - y plane.

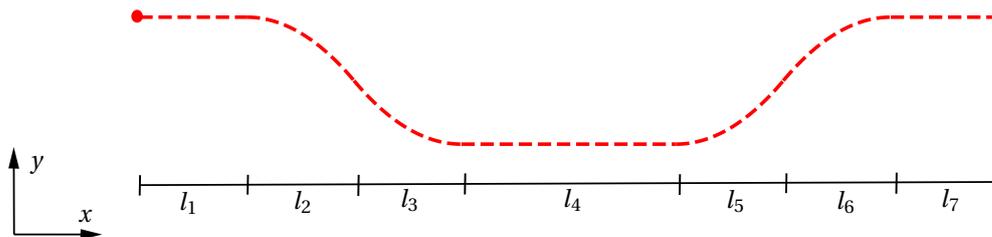


Figure B.2: Schematic of the fiber centerline defined in x - y plane.

The l_1 to l_7 segments' positions are described in x - y mathematics function.

l_1 : This part centerline l_1 is a straight line, the position is $0 \leq x \leq 1, y = 0.1$.

l_2 : This part centerline l_2 is a partial curve of a circle with radius $R = 5.05$, circle center locates at $(1, -4.95)$. Then the position is $1 \leq x \leq 2, y = -4.95 + \sqrt{R^2 - (x-1)^2}$.

l_3 : This part centerline l_3 is a partial curve of a circle with radius $R = 5.05$, circle center locates at $(3, 4.95)$. Then the position is $2 \leq x \leq 3, y = 4.95 - \sqrt{R^2 - (x-3)^2}$.

l_4 : This part centerline l_4 is a straight line, the position is $3 \leq x \leq 5, y = -0.1$.

l_5 : This part centerline l_5 is a partial curve of a circle with radius $R = 5.05$, circle center locates at (5, 4.95). Then the position is $5 \leq x \leq 6$, $y = 4.95 - \sqrt{R^2 - (x - 5)^2}$.

l_6 : This part centerline l_6 is a partial curve of a circle with radius $R = 5.05$, circle center locates at (7, -4.95). Then the position is $6 \leq x \leq 7$, $y = -4.95 + \sqrt{R^2 - (x - 7)^2}$.

l_7 : This part centerline l_7 is a straight line, the position is $7 \leq x \leq 8$, $y = 0.1$.

The other seven fibers positions can also be derived as this example shown.

C

Analytic Effective Heat Conductivity of A Simple Cubic Composite Model

Figure C.1 shows a 3D two material cubic model with heat conductivity κ_1 and κ_2 . The cubic model is split into two cuboid material phase with vertical length l_1 and l_2 . Neumann boundary condition is prescribed on the top surface with heat flux value \bar{q} . The bottom surface is prescribed with Dirichlet condition T_1 . After heat transfer equilibrium, the top surface will end in a temperature T_2 . The temperature in the material interface is set as T_m . Due to the fact that the material interface is a level plane, the above-mentioned temperature are all uniform, which are considered as average temperature in these surfaces. Then with the definition of Neumann boundary condition, we have the following temperature equation

$$T_2 - T_m = \frac{\bar{q} \cdot l_2}{\kappa_2} \quad (\text{C.1a})$$

$$T_m - T_1 = \frac{\bar{q} \cdot l_1}{\kappa_1} \quad (\text{C.1b})$$

$$T_2 - T_1 = \frac{\bar{q} \cdot l}{\kappa_e} \quad (\text{C.1c})$$

Where k_e is the effective heat conductivity of the cubic model, $l = l_1 + l_2$ is the model total vertical length. Equations (C.1a) and (C.1b) are defined in each material phase, and the Equation (C.1c) is defined on the whole model domain. Adding Equations (C.1a) and (C.1b) together, we have $T_2 - T_1 = \bar{q} \left(\frac{l_2}{\kappa_2} + \frac{l_1}{\kappa_1} \right)$, and then comparing it with the Equation (C.1c), the effective heat conductivity of this two material cubic model, $\kappa_e = \frac{\kappa_1 \cdot \kappa_2 \cdot l}{l_2 \cdot \kappa_1 + l_1 \cdot \kappa_2}$, is analytically derived.

With the above analytically derived composite effective heat conductivity equation, the same cubic model is simulated to obtain the temperature field. The numerical effective heat conductivity in z direction is $\kappa_{en} = \frac{50 \times 2}{74 - 10} = 1.5625$, which can be directly obtained by using the Equations (2.28) and (2.29). The corresponding analytic effective heat conductivity is $\kappa_{ea} = \frac{5 \times 1 \times 2}{1 \times 0.9 + 5 \times 1.1} = 1.5625$. These two effective heat conductivity values are the same, which verifies the numerical method to determine the effective heat conductivity of composite model.

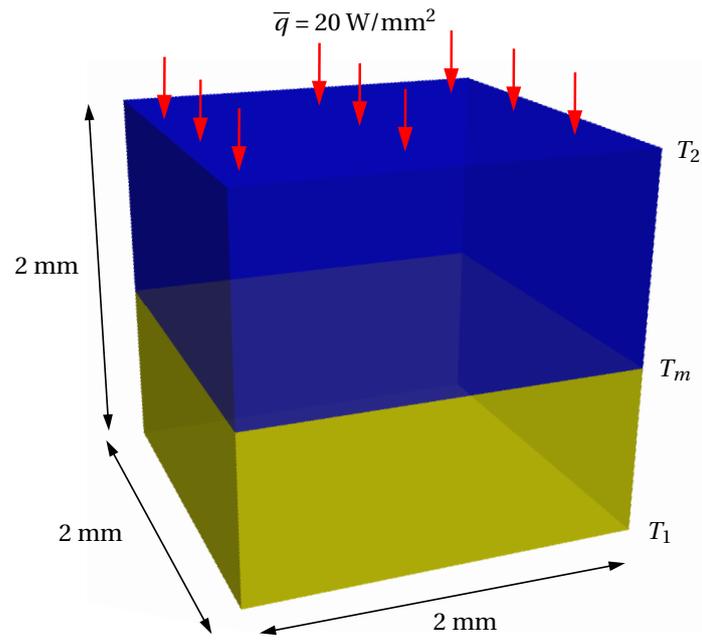


Figure C.1: 3D cubic model for the effective heat conductivity verification problem.

D

The Fiber Volume with A Cosine Function Centerline

In the Representative Volume Element model, there are total eight fibers, each fiber has the same geometry, we then look into one fiber to determine the fiber volume.

The volume of each fiber V_f can be calculated as

$$V_f = AL \quad (\text{D.1})$$

where A is the fiber cross-section area and L is the length of centerline.

The ideal geometry of this model assumes that the centreline position of fiber can be described by a simple trigonometric form

$$z(x) = a \cos\left(\frac{2\pi x}{l_f}\right) \quad (\text{D.2})$$

where a and l_f are the amplitude and wavelength of the fiber, x is the horizontal location in the fiber arbitrary point.

Fiber centerline length L can be calculated by curve integration

$$\begin{aligned} L &= \int_0^l \sqrt{1 + \left(\frac{dz}{dx}\right)^2} dx \\ &= \int_0^l \sqrt{1 + \left[\frac{2\pi a}{l_f} \sin\left(\frac{2\pi x}{l_f}\right)\right]^2} dx \end{aligned} \quad (\text{D.3})$$

Equation (D.3) integral function has no explicit form, which is difficult to integrate using curve integration. But this can be transformed into the second kind complete elliptic integral, defined as

$$\begin{aligned} E(\phi, k) &= \int_0^\phi \sqrt{1 - k^2 \sin^2(\theta)} d\theta \\ &= \frac{\pi}{2} \sum_0^\infty \left(\frac{2n!}{2^{2n}(n!)^2}\right) \frac{k^{2n}}{1-2n} \end{aligned} \quad (\text{D.4})$$

with $\phi \in \left(0, \frac{\pi}{2}\right)$ and $k \in (0, 1)$.

Due to the fact that the curve length of sinusoidal function is equal to cosine function if the amplitude and wavelength are the same. Then Equation (D.3) can be rewritten with the substitution of sinusoidal function

$z'(x) = a \sin\left(\frac{2\pi x}{l_f}\right)$ and the trigonometric identity $\sin^2 \alpha + \cos^2 \alpha = 1$. That is

$$\begin{aligned} L &= \int_0^{l_f} \sqrt{1 + \left[\frac{2\pi b}{l_f} \cos\left(\frac{2\pi x}{l_f}\right)\right]^2} dx \\ &= \int_0^{l_f} \sqrt{1 + \frac{4\pi^2 b^2}{l_f^2} \left[1 - \sin^2\left(\frac{2\pi x}{l_f}\right)\right]} dx \end{aligned} \quad (\text{D.5})$$

Let $\theta = \frac{2\pi x}{l_f}$, $k^2 = \frac{\frac{4\pi^2 a^2}{l_f^2}}{1 + \frac{4\pi^2 a^2}{l_f^2}}$, $dx = \frac{l_f}{2\pi} d\theta$. Defining the variable x varies from 0 to $\frac{l_f}{4}$, or $\frac{1}{4}$ length of the

centerline, then the corresponding value θ domain is $\theta \in [0, \frac{\pi}{2}]$, the length of the centerline with a cosine function can be obtained by standard elliptical integration as follows

$$\begin{aligned} L &= \frac{2}{\pi} \sqrt{l_f^2 + 4\pi^2 a^2} \int_0^{\frac{\pi}{2}} \sqrt{1 - k^2 \sin^2(\theta)} d\theta \\ &= \sqrt{l_f^2 + 4\pi^2 a^2} \sum_0^{\infty} \left(\frac{(2n)!}{2^{2n}(n!)^2} \right) \frac{k^{2n}}{1 - 2n} \\ &= \frac{2}{\pi} \sqrt{l_f^2 + 4\pi^2 a^2} E(\phi, k) \end{aligned} \quad (\text{D.6})$$

Then, with the derived fiber length formula Equation (D.6) and the fiber cross-section area A , the fiber volume can be calculated accordingly.

E

Parameters Mapping of Twill Composite Model Effective Heat Conductivity

The derivations of the effective heat conductivity in the 3D composite model takes long computational time to get the numerical solution. Therefore, in the optimization problem, the involved function evaluations is expensive to conducted, which will pose challenges to the optimization process, specifically for possible global optimization algorithm. To reduce the computation time, here we introduce a parameter mapping scheme to fit data collecting the effective heat conductivity at a few design points, using the principle response surface method and least square method.

As for the optimization problem is this work, the design variables domain are defined as following with the increasing step size $\Delta = 0.025$

$$\begin{cases} a \in [0.5, 1], & \Delta a = 0.025 \\ b \in [0.5, 0.75], & \Delta b = 0.025 \end{cases} \quad (\text{E.1})$$

The design variable combination point is $s = [a, b]$. With Equation (E.1), total $21 \times 11 = 231$ numerical simulations in different s are conducted to get the effective heat conductivity database.

The obtained effective heat conductivity values are stored in each S_i matrix, where $i = 1, 2, 3, \dots, 231$. The effective heat conductivity value matrix is S

$$S = [S_1, S_2, S_2, \dots, S_N]. \quad (\text{E.2})$$

where N is the total number of the numerical simulations.

After the effective heat conductivity database S is obtained. The next step is to establish a parameter mapping relationship between the design variables and effective heat conductivity coefficients. There are two design variables in the optimization problem, a 2-rd polynomial bases P_i with the two design variables combination a_i and b_i is used, which serves to map the effective heat conductivity value with design variables.

$$P_i = [1, a_i, b_i, a_i b_i, a_i^2, b_i^2] \quad (\text{E.3})$$

Then for each effective heat conductivity value S_i , there is a corresponding parameter polynomial base P_i . Considering one effective heat conductivity value S_i , this value can be approximated by the P_i with a weighting coefficient matrix w_α

$$S_i = w_\alpha \cdot P_i + \varepsilon_i \quad (\text{E.4})$$

where ε_i is the approximate error.

When all the values in the S matrix are included, Equation (E.4) can be expanded into

$$\begin{cases} S_1 - w_\alpha \cdot P_1 = \varepsilon_1 \\ S_2 - w_\alpha \cdot P_2 = \varepsilon_2 \\ S_3 - w_\alpha \cdot P_3 = \varepsilon_3 \\ \dots\dots \\ S_N - w_\alpha \cdot P_N = \varepsilon_N \end{cases} \quad (\text{E.5})$$

With the coefficient matrix w_α , ε_i in each sub-equation in Equation (E.5) should to be made as small as possible. By using the least square method, the minimization problem is defined as $f = \sum_i^N (S_i - w_\alpha \cdot P_i)^2$. Let $A = P_i$, $B = S_i$, the expression of w_α matrix solution is

$$w_\alpha = (A^T A)^{-1} A^T B \quad (\text{E.6})$$

After the weighting coefficient matrix w_α is determined, then for arbitrary design point $s_u = [a_u, b_u]$, the corresponding unknown polynomial basis is P_u , the effective heat conductivity of the design point s_u approximation is

$$S_u = w_\alpha \cdot P_u \quad (\text{E.7})$$

With this parameter mapping process, if the database S is well constructed, the effective heat conductivity evaluation of each design point sample can be rapidly performed, and this established method has very high computation efficiency.

To verified the effectiveness of this parameter mapping method, five points $s_1 = [0.515, 0.746]$, $s_2 = [0.753, 0.62]$, $s_3 = [0.99, 0.51]$, $s_4 = [0.503, 0.502]$, $s_5 = [0.985, 0.74]$ locate at the upper, lower and medium values in the design variables domain are compared with both the numerical and parameter mapping results. As Figure E.1 shows, the parameter mapping method can get accurate effective heat conductivity without the heavy computational load. This ability promotes the use the global optimization algorithm involves numerous objective function evaluations in the three dimensional composite model to get the global optimal design.

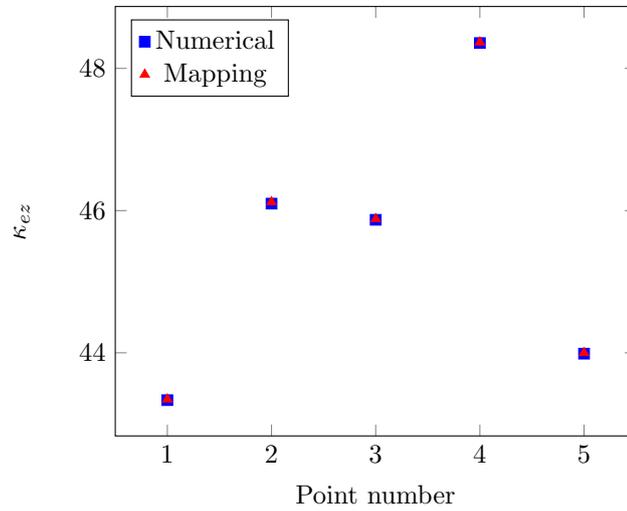


Figure E.1: Numerical example points to verify the effectiveness of the parameters mapping method.

References

- [1] Rana, Sohel, and Raul Figueiro, editors. *Advanced Composite Materials for Aerospace Engineering : Processing, Properties and Applications*. Woodhead Publishing Is an Imprint of Elsevier, 2016.
- [2] Bouhfid, Rachid, et al. *Polymer Nanocomposite-Based Smart Materials: From Synthesis to Application*. Woodhead Publishing, 2020.
- [3] Sheno, R.A, and J.F Wellicome. *Composite Materials in Maritime Structures*. Vol. 2, Practical Considerations, Cambridge University Press, 1993.
- [4] Kobelev, Vladimir. *Design and Analysis of Composite Structures for Automotive Applications : Chassis and Drivetrain*. First edition., First ed., Wiley, 2019.
- [5] Mohammad Zahid, Rajneesh Sharma, et al. "Micro-structurally informed finite element analysis of carbon/carbon composites for effective thermal conductivity." *Composite Structures*, vol. 226, 2019.
- [6] Wang, Yang, et al. "Improved Sandwich Structured Ceramic Matrix Composites with Excellent Thermal Insulation." *Composites part B, Engineering*, vol. 129, 2017, pp. 180–186.
- [7] Ravikovich, Yury, et al. "Application of Composite Materials in an Upgraded Engine Low-Pressure Compressor for a Regional Passenger Aircraft." *Inventions*, vol. 6, no. 3, 2021, pp. 54–54.
- [8] Okereke, M.I, et al. "Virtual Testing of Advanced Composites, Cellular Materials and Biomaterials: A Review." *Composites Part B*, vol. 60, 2014, pp. 637–662.,
- [9] Wang, Hailou, et al. "Numerical Analysis of Thermal Expansion Behaviors and Interfacial Thermal Stress of 3d Braided Composite Materials." *Computational Materials Science*, vol. 138, 2017, pp. 77–91.,
- [10] Naji, Malak, et al. "Thermal Stress Investigation in Unidirectional Composites Under the Hyperbolic Energy Model." *International Journal of Solids and Structures*, vol. 44, no. 16, 2007, pp. 5111–5121.
- [11] Bard S, et al. "Influence of Fiber Volume Content on Thermal Conductivity in Transverse and Fiber Direction of Carbon Fiber-Reinforced Epoxy Laminates." *Materials (Basel, Switzerland)*, vol. 12, no. 7, 2019.
- [12] Liu, Xin, et al. "A Unified Approach for Thermoelastic Constitutive Modeling of Composite Structures." *Composites Part B*, vol. 172, 2019, pp. 649–659.
- [13] Lipcan, Maximilian, et al. "Thermal Response of Frame-Like Composite Structures to Analytically Assess Manufacturing Distortion." *Composites Part A*, vol. 107, 2018, pp. 399–408.
- [14] Mei, Hui, et al. "Effect of Fiber Architectures on Thermal Cycling Damage of C/Sic Composites in Oxidizing Atmosphere." *Materials Science & Engineering A*, vol. 460, 2007, pp. 306–313.
- [15] Yang Z, Yang J. "Investigation of long-term thermal aging-induced damage in oxide/oxide ceramic matrix composites." *Journal of the European Ceramic Society*, vol. 40, 2020, pp. 1549-1556.
- [16] Yan, X. "Finite Element Formulation of a Heat Transfer Problem for an Axisymmetric Composite Structure." *Computational Mechanics -International Journal Then Research Journal-*, vol. 36, no. 1, 2005, pp. 76–82.
- [17] M Nurhaniza, et al. "Finite Element Analysis of Composites Materials for Aerospace Applications." *Iop Conference Series: Materials Science and Engineering*, vol. 11, no. 1, 2010.
- [18] Qian, Lijia, et al. "Theoretical Model and Finite Element Simulation on the Effective Thermal Conductivity of Particulate Composite Materials." *Composites Part B*, vol. 116, 2017, pp. 291–297.
- [19] Fries, Thomas-Peter, and Ted Belytschko. "The Extended/Generalized Finite Element Method: An Overview of the Method and Its Applications: The GEFM/XFEM: An Overview of the Method." *International Journal for Numerical Methods in Engineering*, vol. 84, no. 3, 2010, pp. 253–304.
- [20] Wu, Jiale, et al. "Analysis of the Heat Conduction Mechanism for Al₂O₃/Silicone Rubber Composite Material with Fem Based on Experiment Observations." *Composites Science and Technology*, vol. 210, 2021.

- [21] Armero, Francisco, et al. "Brittle Fracture in Polycrystalline Microstructures with the Extended Finite Element Method: Brittle Fracture in Polycrystalline Microstructures with the X-Fem." *International Journal for Numerical Methods in Engineering*, vol. 56, no. 14, 2003, pp. 2015–2037.
- [22] Melenk, J.M, and Babuška I. "The Partition of Unity Finite Element Method: Basic Theory and Applications." *Computer Methods in Applied Mechanics and Engineering*, vol. 139, no. 1, 1996, pp. 289–314.
- [23] O'Hara, P, et al. "Generalized Finite Element Analysis of Three-Dimensional Heat Transfer Problems Exhibiting Sharp Thermal Gradients." *Computer Methods in Applied Mechanics and Engineering*, vol. 198, no. 21, 2009, pp. 1857–1871.
- [24] O'Hara, P, et al. "Efficient Analysis of Transient Heat Transfer Problems Exhibiting Sharp Thermal Gradients." *Computational Mechanics : Solids, Fluids, Structures, Fluid-Structure Interactions, Biomechanics, Micromechanics, Multiscale Mechanics, Materials, Constitutive Modeling, Nonlinear Mechanics, Aerodynamics*, vol. 51, no. 5, 2013, pp. 743–764.
- [25] Abbas, Safdar, et al. "The Xfem for High-Gradient Solutions in Convection-Dominated Problems." *International Journal for Numerical Methods in Engineering*, vol. 82, no. 8, 2010, pp. 1044–1072.
- [26] Waisman, Haim, and Ted Belytschko. "Parametric Enrichment Adaptivity by the Extended Finite Element Method." *International Journal for Numerical Methods in Engineering*, vol. 73, no. 12, 2008, pp. 1671–1692.
- [27] Zeller, Christian, et al. "Parameterized Extended Finite Element Method for High Thermal Gradients." *Journal of Computational Design and Engineering*, vol. 5, no. 3, 2018, pp. 329–336.
- [28] Iqbal, M, et al. "Local Adaptive Q -Enrichments and Generalized Finite Elements for Transient Heat Diffusion Problems." *Computer Methods in Applied Mechanics and Engineering*, vol. 372, 2020.
- [29] Soghrati, Soheil, et al. "An Interface-Enriched Generalized Fem for Problems with Discontinuous Gradient Fields: Interface-Enriched Gfem." *International Journal for Numerical Methods in Engineering*, vol. 89, no. 8, 2012, pp. 991–1008.
- [30] Aragón Alejandro M, et al. "Effect of In-Plane Deformation on the Cohesive Failure of Heterogeneous Adhesives." *Journal of the Mechanics and Physics of Solids*, vol. 61, no. 7, 2013, pp. 1600–1611.
- [31] Zhang, Xiang, et al. "Igfem-Based Shape Sensitivity Analysis of the Transverse Failure of a Composite Laminate." *Computational Mechanics*, vol. 64, no. 5, 2019, pp. 1455–1472.
- [32] Shakiba, Maryam, et al. "Transverse Failure of Carbon Fiber Composites: Analytical Sensitivity to the Distribution of Fiber/Matrix Interface Properties." *International Journal for Numerical Methods in Engineering*, vol. 120, no. 5, 2019, pp. 650–665.
- [33] Tan M.H.Y, and Geubelle P.H. "3d Dimensionally Reduced Modeling and Gradient-Based Optimization of Microchannel Cooling Networks." *Computer Methods in Applied Mechanics and Engineering*, vol. 323, 2017, pp. 230–249.
- [34] Van den Boom, S. J, et al. "An Interface-Enriched Generalized Finite Element Method for Level Set-Based Topology Optimization." *Structural and Multidisciplinary Optimization*, vol. 63, no. 1, 2021, pp. 1–20.
- [35] Soghrati, S, and P. H Geubelle. "A 3d Interface-Enriched Generalized Finite Element Method for Weakly Discontinuous Problems with Complex Internal Geometries." *Computer Methods in Applied Mechanics and Engineering*, 217/220, 2012, pp. 46–57.
- [36] Soghrati, Soheil, et al. "Computational Analysis of Actively-Cooled 3d Woven Microvascular Composites Using a Stabilized Interface-Enriched Generalized Finite Element Method." *International Journal of Heat and Mass Transfer*, vol. 65, 2013, pp. 153–164.
- [37] Tan, Marcus H.Y, et al. "A Nurbs-Based Interface-Enriched Generalized Finite Element Scheme for the Thermal Analysis and Design of Microvascular Composites." *Computer Methods in Applied Mechanics and Engineering*, vol. 283, 2015, pp. 1382–1400.

- [38] Aragón, Alejandro M, et al. "On the Stability and Interpolating Properties of the Hierarchical Interface-Enriched Finite Element Method." *Computer Methods in Applied Mechanics and Engineering*, vol. 362, 2020.
- [39] Guo, Yongqiang, et al. "Factors Affecting Thermal Conductivities of the Polymers and Polymer Composites: A Review." *Composites Science and Technology*, vol. 193, 2020.
- [40] Burger, N, et al. "Review of Thermal Conductivity in Composites: Mechanisms, Parameters and Theory." *Progress in Polymer Science*, vol. 61, 2016, pp. 1–28.
- [41] Gori, F, et al. "Theoretical Prediction of Thermal Conductivity for Thermal Protection Systems." *Applied Thermal Engineering*, vol. 49, 2012, pp. 124–130.
- [42] Gou, Jian-Jun, et al. "Numerical Study of Effective Thermal Conductivities of Plain Woven Composites by Unit Cells of Different Sizes." *International Journal of Heat and Mass Transfer*, vol. 91, 2015, pp. 829–840.
- [43] Zhou, Xiao-Yi, et al. "Design Optimization for Thermal Conductivity of Plain-Woven Textile Composites." *Composite Structures*, vol. 255, 2021.
- [44] Yan, Biaojie, et al. "Optimization of Thermal Conductivity of UO₂-Mo Composite with Continuous Mo Channel Based on Finite Element Method and Machine Learning." *International Journal of Heat and Mass Transfer*, vol. 159, 2020.
- [45] He Liu, Mengyao Hu, et al. "Geometric optimization of aerogel composites for high temperature thermal insulation applications." *Journal of Non-Crystalline Solids*, Volume 547, 2020.
- [46] Yin, Zhenyuan, et al. "Estimation of the Thermal Conductivity of a Heterogeneous CH₄-Hydrate Bearing Sample Based on Particle Swarm Optimization." *Applied Energy*, vol. 271, 2020.
- [47] Moës Nicolas, et al. "Imposing Dirichlet Boundary Conditions in the Extended Finite Element Method." *International Journal for Numerical Methods in Engineering*, vol. 67, no. 12, 2006, pp. 1641–1669.
- [48] Babuška Ivo, et al. "Survey of Meshless and Generalized Finite Element Methods: A Unified Approach." *Acta Numerica*, vol. 12, no. 1, 2003, pp. 1–125.
- [49] Aragón Alejandro M, et al. "Generalized Finite Element Enrichment Functions for Discontinuous Gradient Fields." *International Journal for Numerical Methods in Engineering*, vol. 82, no. 2, 2010, pp. 242–268.
- [50] Cheney, Ward. "The Chain Rule and Mean Value Theorems". *Analysis for Applied Mathematics*. New York: Springer. 2001, pp. 121–125.
- [51] Moës N, et al. "A Computational Approach to Handle Complex Microstructure Geometries." *Computer Methods in Applied Mechanics and Engineering*, vol. 192, no. 28, 2003, pp. 3163–3177.
- [52] Fries, Thomas-Peter. "A Corrected Xfem Approximation Without Problems in Blending Elements." *International Journal for Numerical Methods in Engineering*, vol. 75, no. 5, 2008, pp. 503–532.
- [53] Bakalakos, Serafeim, et al. "An Extended Finite Element Method Formulation for Modeling Multi-Phase Boundary Interactions in Steady State Heat Conduction Problems." *Composite Structures*, vol. 258, 2021.
- [54] Stable GFEM (SGFEM): Gupta, V, et al. "Stable Gfem (Sgfem): Improved Conditioning and Accuracy of Gfem/Xfem for Three-Dimensional Fracture Mechanics." *Computer Methods in Applied Mechanics and Engineering*, vol. 289, 2015, pp. 355–386.
- [55] Belytschko, T, et al. "Arbitrary Discontinuities in Finite Elements." *International Journal for Numerical Methods in Engineering*, vol. 50, no. 4, 2001, pp. 993–1013.
- [56] Ko, Kwanghee, and Takis Sakkalis. "Orthogonal Projection of Points in Cad/Cam Applications: An Overview." *Journal of Computational Design and Engineering*, vol. 1, no. 2, 2014, pp. 116–127.
- [57] Wang, Michael Yu, and Xiaoming Wang. "'Color' Level Sets: A Multi-Phase Method for Structural Topology Optimization with Multiple Materials." *Computer Methods in Applied Mechanics and Engineering*, vol. 193, no. 6-8, 2004, pp. 469–496.

- [58] Jiang, Long, et al. "Parametric Shape and Topology Optimization: A New Level Set Approach Based on Cardinal Basis Functions." *International Journal for Numerical Methods in Engineering*, vol. 114, no. 1, 2018, pp. 66–87.
- [59] Islam, Md, and A Pramila. "Thermal Conductivity of Fiber Reinforced Composites by the Fem." *Journal of Composite Materials*, vol. 33, no. 18, 1999, pp. 1699–1715.
- [60] Alger, Mark S. M. *Polymer Science Dictionary*. Third edition., Third ed., Springer, 2017.
- [61] Rao, Singiresu S. *Engineering Optimization : Theory and Practice*. Fourth edition., Fourth ed., John Wiley & Sons, 2009.
- [62] Lv, Honglin, et al. "Optimization of Micromixer with Cantor Fractal Baffle Based on Simulated Annealing Algorithm." *Chaos, Solitons and Fractals: The Interdisciplinary Journal of Nonlinear Science, and Nonequilibrium and Complex Phenomena*, vol. 148, 2021.